Final Technical Report – RPTXXXX

Project Title: High Efficiency PEM Water Electrolysis Enabled by Advanced Catalysts, Membranes and Processes

Project Period of Performance: September 1st, 2017 – February 28th, 2021

Project Reporting Final: 09/01/2017 to 02/28/2021

Date of Report: 02/07/2023

Recipient: Proton Energy Systems d/b/a Nel Hydrogen US

Working Partners: University of California Irvine (UCI), Oak Ridge National Laboratory, HydroGEN EMN National Lab Consortium

Contact:
PI: Katherine Ayers
Co-PI: Chris Capuano
Business Contact: Stephen Szymanski

DOE Managers:
Technology Manager: David Peterson
Project Engineer: Kim Cierpik-Gold

Acknowledgment: "This material is based upon work supported by the U.S. Department of Energy's Office of Energy Efficiency and Renewable Energy (EERE) under the Hydrogen & Fuel Cell Technologies Office (HFTO) Award Number DE-EE0008081".

Table of Contents

Executive Summary:

In this project, advanced membranes and catalysts were integrated into membrane electrode assembles (porous transport electrodes (PTE) or catalyst coated membranes (CCM)) leveraging precision coating methods to enable control of electrode structures and demonstration of the best component performance possible with these materials. Partner collaborations allowed for advanced characterization of the formed interfaces and degradation mechanisms. New methods of forming hydrogen recombination layers were also developed, to move away from wet chemistry processes that would have limited realization and implementation of the optimized electrode configurations in a commercial environment.

Key results included successful testing of hydrogen recombination layers developed and fabricated at Nel with initial achievement of the 75% effectiveness milestone. A "dry" type deposition built on these results to achieve 87% effectiveness in full turndown. A 2-cell durability test was completed using a sub-scale 86 cm^2 design, based on the Nel's MW scale platform. A 50-micron membrane demonstrated an ~66% reduction in membrane thickness versus the current commercial design at Nel, while the PGM content of 0.7 mg/cm^2 represents a ~80% reduction in catalyst without impact to voltage stability.

All milestones were completed including the final program milestone demonstrating activity and 500 hr durability of advanced MEA in 3-cell 86 cm^2 electrolysis stack. This stack met all the project specific targets given in Table 1 below including exceeding the durability target and achieving 1500 hrs of operation. A manuscript was submitted related to OER catalyst activity and degradation studies by the National Renewable Energy Lab (NREL) and a second was submitted for different PTE vs CCM loading and interfacial analysis by University of California Irvine.

Project Objective:

Proton Energy Systems d/b/a Nel Hydrogen US has developed an advanced proton exchange membrane water electrolysis (PEMWE) membrane electrode assembly (MEA) that meets or exceeds the EMN targets by addressing membrane, catalyst, catalyst layers and their interfaces. To accomplish this advancement, we have leveraged our expertise in proton exchange membrane water electrolysis (PEMWE) and previously funded DOE work, partnered with experts in the field University of California, Irvine (UCI) and Oak Ridge National Laboratory and heavily leveraged EMN resources. The objective of this project was to develop a high TRL advanced electrolysis MEA that can meet the following targets: produce H_2 at 43 kWh/kg, with decay rates of less than 4 mV/1000 h and at costs of $2 /kg H_2 based on $0.02/kWh renewable energy input as estimated by the H2A model.

Background:

Proton/Nel is a world leader in PEM electrolysis, having been in the industry for 20 years and with the largest market share of PEM systems in the field. The core technology is derived from General Electric (GE) and United Technologies (UTC), originally used in life support applications, and historically has been highly over-engineered and under-optimized for manufacturing. Based on cost reduction to date, PEM electrolysis systems are profitable and competitive when fielded today for H_2 industrial gas applications and markets. However, for energy storage, H_2 fueling and commodity H_2, the price point of > $5.5/kg H_2 and low efficiency of >50 kWh/kg are unacceptable (see **Table 1**). The cost and efficiency drivers are: i) thick membranes (7-10 mil thick) to prevent excessive gas crossover and seal against 30-350 bar differential pressure, but causing high resistive efficiency losses; ii) high catalyst loadings using conventional low surface area, unsupported catalysts increasing cost and decreasing efficiency; iii) manufacturing for electrode

gas diffusion and porous transport layers (GDL and PTL respectively) that is not optimized for activity, durability, or cost; and iv) low temperature operation due to membrane creep over long lifetimes at higher temperature, which again limits efficiency. Nel has performed early feasibility work to address all four areas, but to demonstrate the improvements in cost and efficiency, additional understanding of materials interactions and electrode structure is needed. Demonstration and integration of these requires a deeper understanding of the scientific and technical aspects of electrolysis-specific membranes, water distribution issues, GDL and catalyst layer interfaces, requiring partners who are experts in the field: UCI and ORNL.

Specification	Proton State of the Art	Proton Lab Demonstrated	Specific FOA Targets
Membrane (μm)	178	50	50
Temperature (°C)	58	80	90
Total catalyst loading (mg/cm^2)	3	1.3	0.9
Durability (mV/1000hrs)	~0	7	4
Efficiency (kWh/kg)	53	44	43
Total Cost H_2 ($/kg H_2)	5.41	2.25	<2
TRL	10	3/4	6

Table 1: Technical targets of the proposal

Task 1: Membrane Characterization

Compression and SAXS experiments

A set of eight samples shown in Table #2 were selected to represent the largest range of material properties for characterization. This set comprised two different chemistries, four different thickness and each sample was tested with and without recombination treatment for hydrogen cross-over. For comparison, the baseline material for this test would be N1110, since this is the current membrane being used in the majority of our commercial systems at the time of this report. The samples were received in liquid-equilibrated form and immersed in liquid water to preserve their equilibrium state. For SAXS experiments, the samples were cut and placed in solution cells with liquid water without disrupting the equilibrium state. The samples were kept liquid-equilibrated prior to, and during, the scattering experiments to eliminate contamination and exposure to air. For compression experiments, a custom-made compression apparatus with a liquid water chamber is attached to an Instron testing machine. First, the sample was cleaned of its excess surface water to ensure contact between the plates and placed into the compression fixture, which was then filled with DI water. The sample was compressed at 10 μm/min up to 35 MPa of compressive stress (over 5,000 psi). This technique allows in-situ measurement of the compressive response of the membrane in liquid water. The experimental results are summarized below in **Table 2**.

Results

Membrane	Description	Notes	Chemistry	Pretreatment Condition	Thickness (nominal, dry)	Thickness (liquid, wet)
					(micrometer)	
N1110	Nafion	Commercial	Long side-chain	**100C**	250	302
N117	Nafion	Commercial	Long side-chain	**100C**	175	211

Membrane	Description	Notes	Chemistry	Pretreatment Condition	Thickness (nominal, dry)	Thickness (liquid, wet)
					(micrometer)	
S90	Solvay	Commercial	Short side-chain	**100C**	90	105
S50	Solvay	Commercial	Short side-chain	**100C**	50	71
N1100 - P	Nafion	Processed	Long side-chain	**100C**	250	309
N117 - P	Nafion	Processed	Long side-chain	**100C**	175	210
S90 - P	Solvay	Processed	Short side-chain	**100C**	90	118
S50 - P	Solvay	Processed	Short side-chain	**100C**	46	51

Table 2. List of membranes investigated in this task properties. Thicknesses of the membranes in hydrated state were measured at LBNL.

Key Findings: Compression Studies

- The membranes exhibit a nonlinear stress-strain response with distinct deformation regimes from low to high (strains and stresses). All the membranes samples could withstand pressures exceeding 35 MPa (5000 psi). (**Figure 1**)
- Strains are calculated from displacement change under compression with respect to the membranes initial (hydrated) thickness. This way, thickness variations between membranes are normalized which enables their comparison.
- The moduli of the membranes calculated at various points on the stress-strain curve increases as the membrane is strained (or pressurized), indicating strain-hardening behavior. This tensile behavior is similar to that of membranes, but with a stronger increase in compression.
- In addition, the moduli of membrane decrease for thinner membranes and with shorter side-chain and lower EW. Since some of these changes occur concurrently (i.e., moving from Nafion to Solvay changes all of these three properties), it is difficult to assess the parameters controlling the compression behavior of the membranes. Measurement of N1035 to get an intermediate point will be considered.
- At lower pressure levels (10 MPa), the variability in data between the Nafion and Solvay makes it difficult to draw conclusions in terms of their mechanical response. (**Figure 2**)
- At higher pressure levels (30 MPa), baseline membranes exhibit a trend of increased strain (relative deformation) with reduced membrane thickness (From Nafion 1110 to Solvay 90), with a notable exception of Solvay 50.
- In addition, the effect of processing on Nafion membrane is rather small (within ±10 %), whereas the effect of processing on deformability is more pronounced for Solvay membranes. (**Figure 3**)

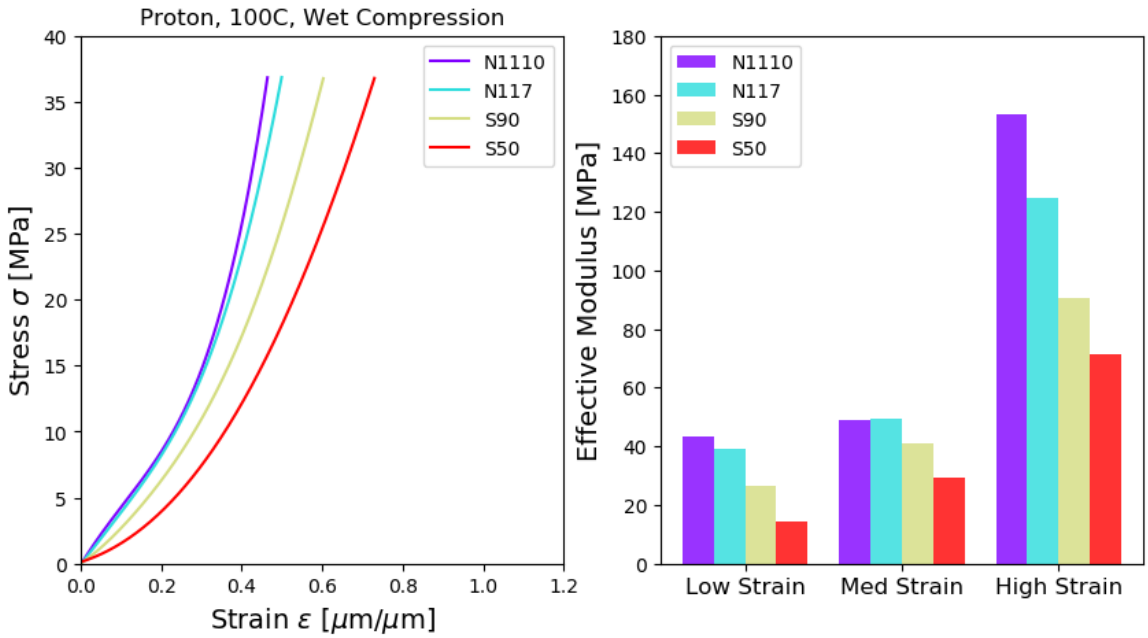

Figure 1 Stress-strain response of four polyfluorosulfonic acid (PFSA) membranes under compression in liquid water (left). Modulus of the stress-strain curves determined at three different deformation regimes, from low strain to high strains.

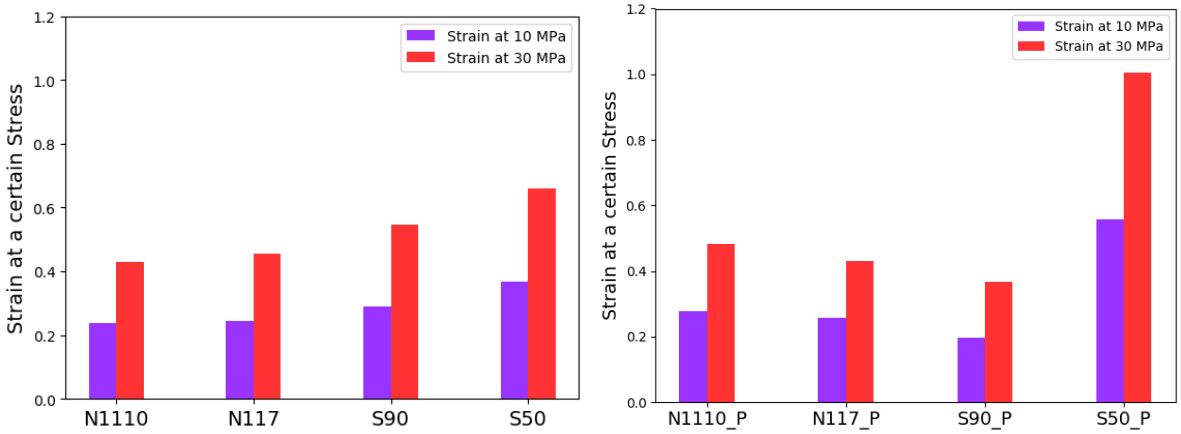

Figure 2 Strain calculated as the relative compression in thickness with respect to initial uncompressed state shown for baseline (left) and processed (right) membranes of four chemistry-thickness types.

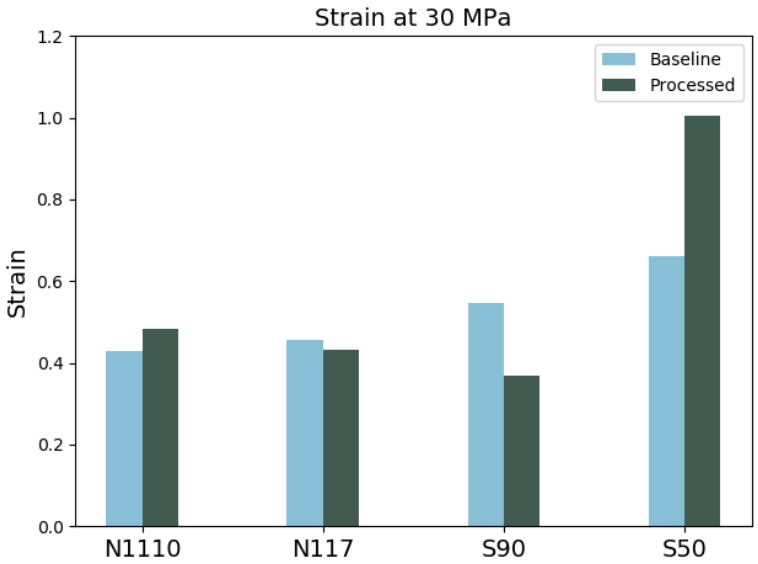

Figure 3 Comparison of compressive strain at 30 MPa pressure for baseline and processed membranes.

Preliminary Findings: Small-angle X-ray scattering (SAXS) Studies

Beam time was available for select experiments to show feasibility of using the beam line to get additional sample information on the internal structure of the membrane samples. This information is invaluable to inform the ex-situ mechanical measurements. Based on those measurements we found that the domain spacing (of hydrophilic domains) in wet state is lower for short side chain (SSC) PFSA compared to that for long side chain (LSC) PFSA (Nafion), in agreement with our previous findings. The d-spacing does not appear to change with processing. However, the small-angle upturn and slope of the intensity profile ($q < 0.01$) corresponding to the correlation lengths of higher than 20 nm changes dramatically. While the origin of such changes is yet to be investigated, it is clear from the preliminary data that processing might alter the morphology at different length scales than at nanoscales (i.e., ionomer domains of 5-6 nm), which could be related to changes in selective transport of certain species.

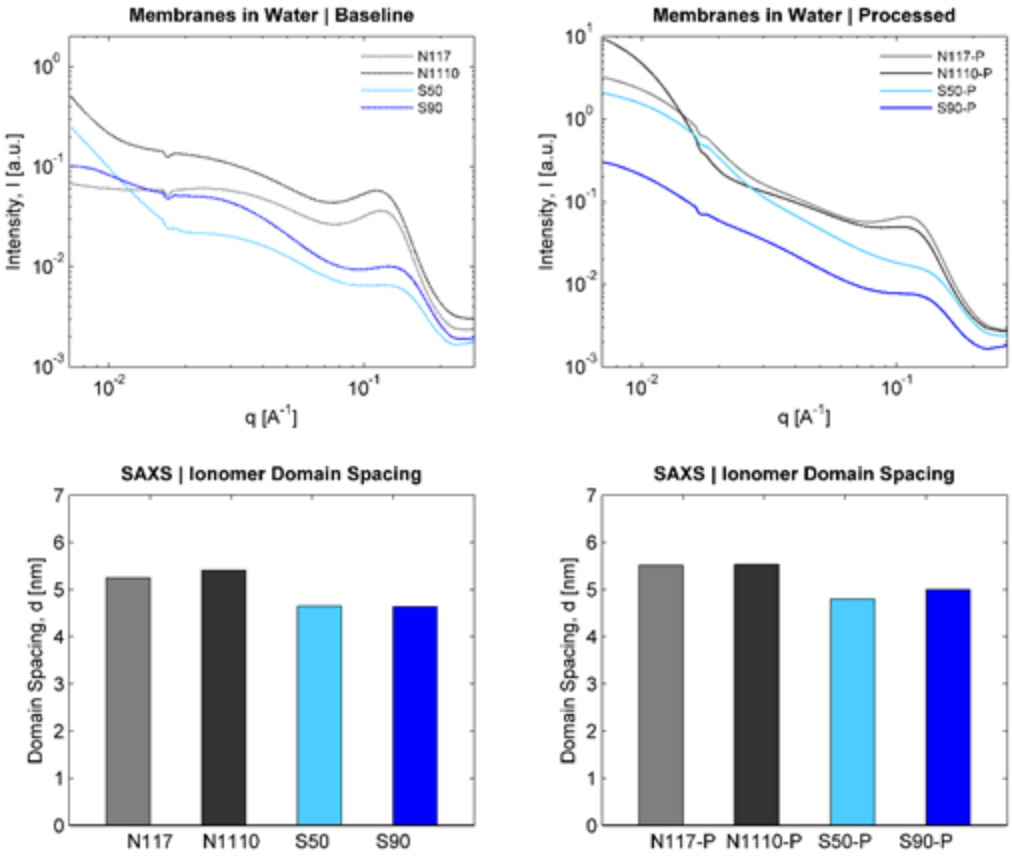

Figure 4 SAXS data of membranes in liquid water (top) and the corresponding domain spacing of the ionomer (below) for baseline (left) and processed (right) membranes.

Compression of PFSA membranes which were purely hydrated were compared vs membranes which were hydrated and had hydrogen cross-over mitigation added as a post-processing step. Materials provided by Proton to LBL to date are shown in **Table 3**. The following were the findings of this analysis.

- The membranes exhibit a nonlinear stress-strain response with distinct deformation regimes and could withstand pressures exceeding 35 MPa (5000 psi).
- At higher pressure levels (30 MPa), baseline membranes exhibit a trend of increased strain (relative deformation) with reduced membrane thickness (from Nafion 1110 to Solvay 90).
- The effect of processing on Nafion membranes is rather small (within ±10 %), but more pronounced for Solvay membranes.

Membrane	Notes	Chemistry	Pretreatment Condition	Thickness (dry) µm	Thickness (liquid) µm
N1110	Commercial	Long side-chain	**100C**	250	302
N117	Commercial	Long side-chain	**100C**	175	211
S90	Commercial	Short side-chain	**100C**	90	105
N1100 - P	Processed	Long side-chain	**100C**	250	309.60
N117 - P	Processed	Long side-chain	**100C**	175	210.25
S90 - P	Processed	Short side-chain	**100C**	90	118.20

Table 3. List of membranes investigated in this project.

Additional activities focused on the design of a heating stage, which was recently completed. Machining of this component is currently in progress. Compression experiments with rate effects were completed for Nafion 117 membrane. Stress-strain data was acquired at three different rates, in liquid water. Results indicated a negligible impact of strain rate on stress-strain response and modulus, especially at the low strain test point shown in **Figure 5**.

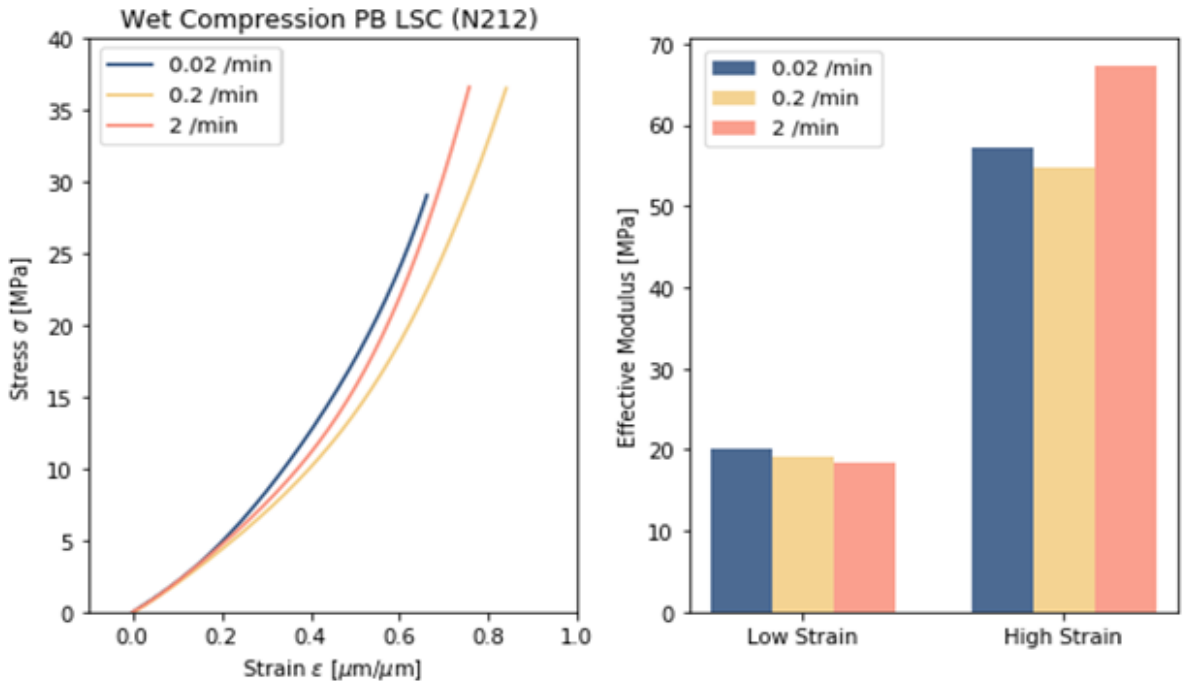

Figure 5. Effect of strain rate on compressive stress-strain response of preboiled Nafion 117 membranes in liquid water at room temperature, 25°C (left). Modulus calculated from the stress-strain curves at low and high strains (right).

Task 2: Advanced MEA Fabrication

Subtask 2.1 Catalyst Layer Fabrication and Characterization

Key Findings: MEA Fabrication

- X-Over treatment on 50 micron membrane produced >80% effectiveness of hydrogen back-diffusion recombination
    - 1000 hrs accumulated on test parts with no loss in durability from treatment
- UCI also developed a tool to visualize oxygen distribution within the PTL.
    - Plots indicate that oxygen forms preferential pathways for transport and that the pathways do not change significantly with the change in water flowrate.
- Both sintered and fiber PTLs show very similar oxygen content in the channel indicating that their mass transport is quite similar

Xover6 and Xover7 build upon previous efforts but represent a process modification allowing for direct coating onto a dry membrane surface or lamination on a dry membrane surface, as opposed to previous efforts where a hydrated membrane was used. This method will allow for easier integration into future manufacturing processes, such as roll-to-roll continuous manufacture, required to further reduce labor content of the finished MEAs. Similarly, a recombination layer was fabricated by depositing recombination layers directly onto the anode side of the membrane through a spray deposition process. A single cell, 100 cm^2 stack was assembled with gas diffusion electrodes (GDEs) to operationally verify the effectiveness of this layer. This test was assessed by cross-over effectiveness before the start of steady state testing. **Table 4** shows the configurations evaluated.

Test	Membrane	Cross-over Layer	Notes
Xover1	7-mil	Baseline	
Xover2	50µm	Baseline	
Xover3	50µm	4x loading	• Pre-hydrated membrane before deposition
Xover4	50µm	4x loading	• No hydration of membrane prior to deposition • Deposited recombination layer, then coated with ionomer in 2-step process
Xover5	50µm	4x loading	• No hydration of membrane prior to deposition • Operated under steady-state conditions, then retested for effectiveness • Deposited blended recombination layer and ionomer in 1-step process
Xover6	50 µm	4x loading	• Recombination layer applied directly to membrane in spray coat process • Membrane is left in “dry” state, allowing for easy integration with roll-to-Roll electrode fabrication process
Xover7	50 µm	4x loading	• Recombination layer transferred to membrane with electrode using common fabrication technique. Consolidates processes into single equipment • Membrane is left in “dry” state, allowing for easy integration with roll-to-Roll electrode fabrication process

Table 4. Hydrogen mitigation test configuration (Blue highlight are new)

The test was operated at 160 amps (1.86 A/cm^2) for a day to reach steady state. At full current, the lower flammability limit (LFL)% values and permeation data were collected, while hydrogen differential pressure was held at 400 psi. The cell stack current was then turned down in two steps of reduced current, thereby reducing the amount of oxygen generated. This allows the operator to see how well the recombination layer is working to scavenge the hydrogen diffusing through the membrane. The results from this test are shown in **Figure 6**. While all three turndown conditions are used to correlate relative performance, the low current value is the most critical, since the absolute hydrogen concentration is the highest at low current when unmitigated.

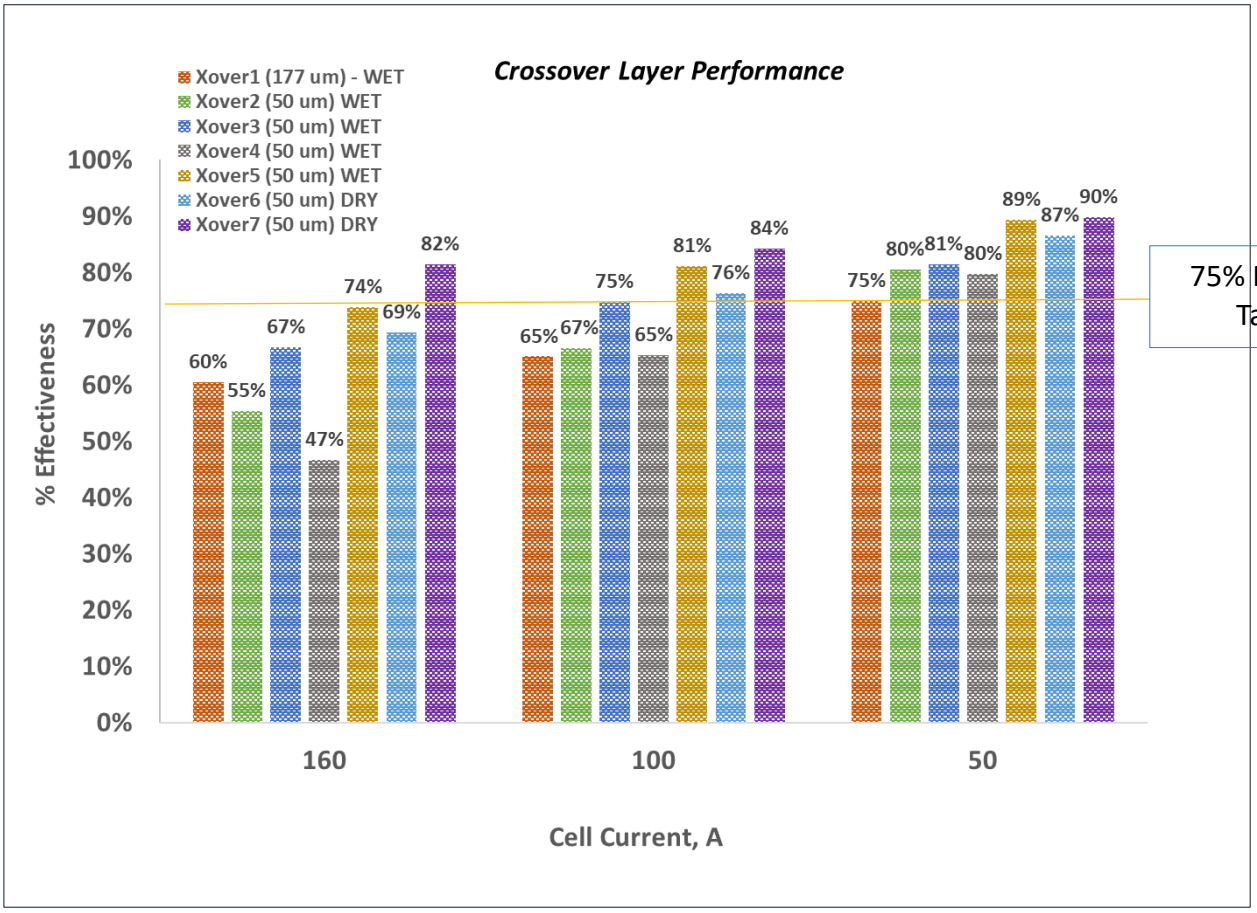

Figure 6. LFL% and percentage of recombination effectiveness at full turndown

As shown in the data above which highlights the most recent test, at full turndown current of 50 amps, the new process applied in the Xover7 sample was able to achieve 90% effectiveness at full turndown, even with membrane thickness of 50 µm membrane. This thickness reduction represents almost 66% versus the 7-mil baseline. The ability to go to this thickness will translate directly into both an operating efficiency improvement, by dropping the ohmic resistance, as well as a CapEx reduction associated with the material reduction.

In addition to the new recombination direct coating approach tests and reported above, a durability test was conducted on the configuration in a separate durability test using the same 100 cm^2 cell configuration sued for the recombination tests discussed above. As shown in previous reports, this layer was also shown to be effective and was combined with work conducted in parallel, specific to electrode ink development and membrane attachment to form a full CCM. Efforts to reduce catalyst loadings through an alternative coating process were explored and applied to the most recent stability tests. Using a Mayer rod coating technique, electrodes were formed using a combined PGM reduction of ~80%. The purpose of the extended test shown below was to evaluate the durability of the cross-over layer, in combination with the lower loaded electrodes, in an operating profile expected from a commercial device. As shown in **Figure 7**, the cell has accumulated over 1000 hrs, with a shown stable voltage under the new configuration. This stability indicates that the addition of the cross-over layer did not introduce new factors that could have changed the degradation rate, as well as the significant catalyst loading reductions.

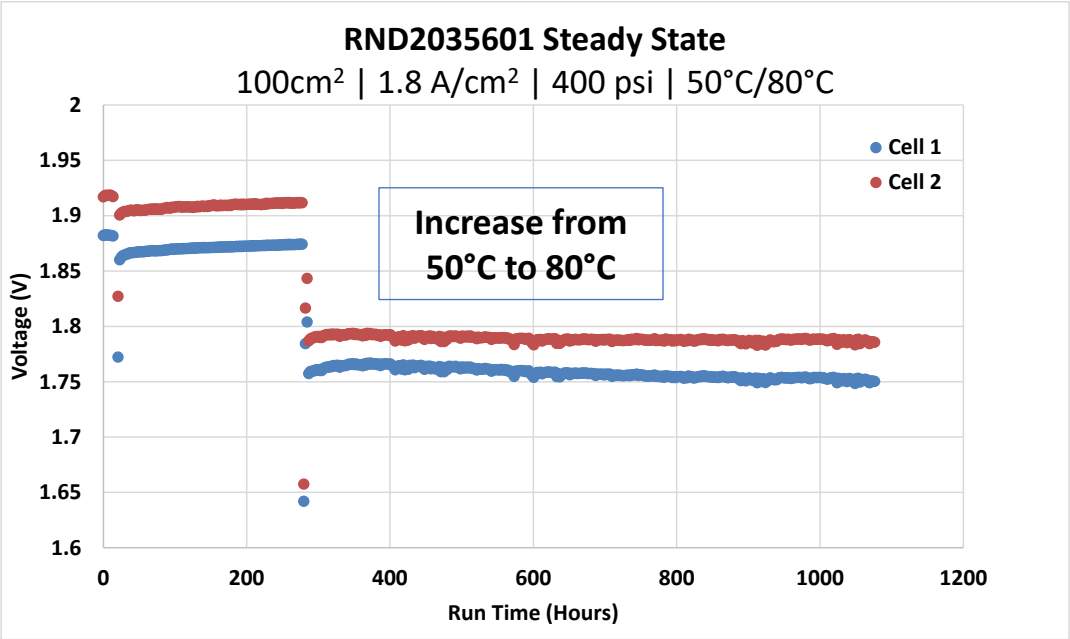

Figure 7. Steady-state data for full CCM test

University of California Irvine (UCI) focused on the following characterization tasks: a) Perform experiments at the Advanced Light Source (ALS) with sets of materials from Nel and conduct data analysis b) Prepare a manuscript from beamtime, c) Submit the final revision to the first journal publication and succeeded in getting the manuscript published. Results are summarized below.

Subtask 2.2 Interface Characterization

The experiments were conducted at the Advanced Photon Source (APS) and the data from (ALS) beamtime was analyzed analysis. This time UCI machined 5 micro-CT electrolyzers, so they could precondition the cells at UCI and ensure that they are operational. **Figure 8** shows 4 machined and assembled electrolyzers.

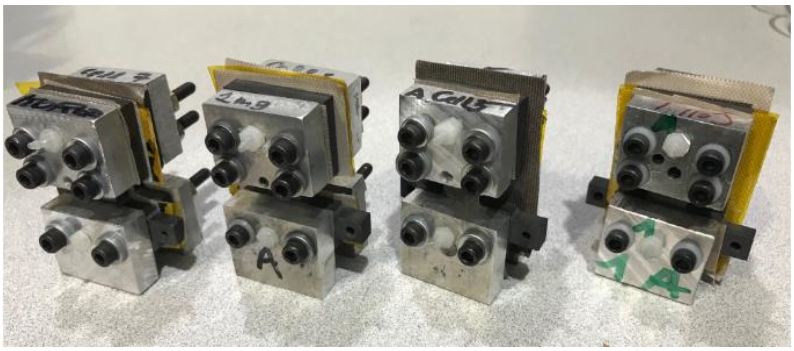

Figure 8. Photograph of assembled 4 electrolyzers that are ready for imaging.

The focus of these experiments was to continue to understand the role of interfaces in PEMWE. For this beamtime UCI compared 6 CCMs and 6 PTEs with three different loadings (0.5, 1, and 2 mg/cm^2 of IrOx), and tested two PTL options (fiber or sintered) to look at the interface of each. UCI imaged the electrolyzer operation in tomography and radiography mode (for oxygen transport properties) and collected polarization curves and constant current hold experiments.

Figure 9 shows polarization curves for fiber and sinter PTEs at three loadings. From **Figure 9a** the electrolyzer with 1.75 mg/cm^2 anode loading has the lowest potential up until 1.4 A/cm^2, however at 1.5 A/cm^2 UCI observed unusual voltage behavior. Further analysis of radiography data will be conducted to understand the origin of this knee in the polarization curve. **Figure 9b** shows polarization curves for sinter PTE at 1.1 and 0.65 mg/cm^2. 0.65 mg/cm^2 shows lower potentials for a given current density, indicating that with sinter PTEs we can go down in loading to 0.65 mg/cm^2. It was unusual that the higher loaded cell did not perform as well, but it is speculated that the non-optimized electrode with higher loadings has lower catalyst utilization because of its thicker and more tightly packed structure. This limits accessibility of the reactants to catalyst sites.

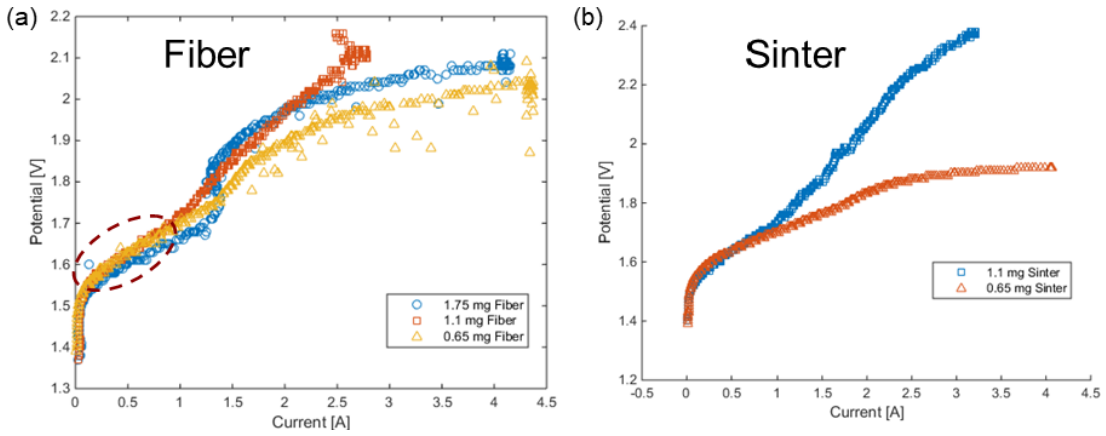

Figure 9. Polarization curves from ALS beamtime comparing a) fiber and b) sinter PTEs at three loadings.

Figure 10 shows polarization curves comparing sintered and fiber PTEs to each other. From **Figure 10a** it is evident that with low loading (0.65 mg/cm^2) anode sinter PTEs show lower potential above 1.5 A/cm^2 compared to fiber PTEs. This might be due to catalyst distribution at the membrane-PTE interface. **Figure 10b** shows PTEs performance for a higher-loaded PTEs with 1.1 mg/cm^2 IrOx loading on the anode. In this scenario both fiber and sinter PTEs showed similar voltage up until 1.7 A/cm^2 but at higher current densities fiber PTE showed lower potential.

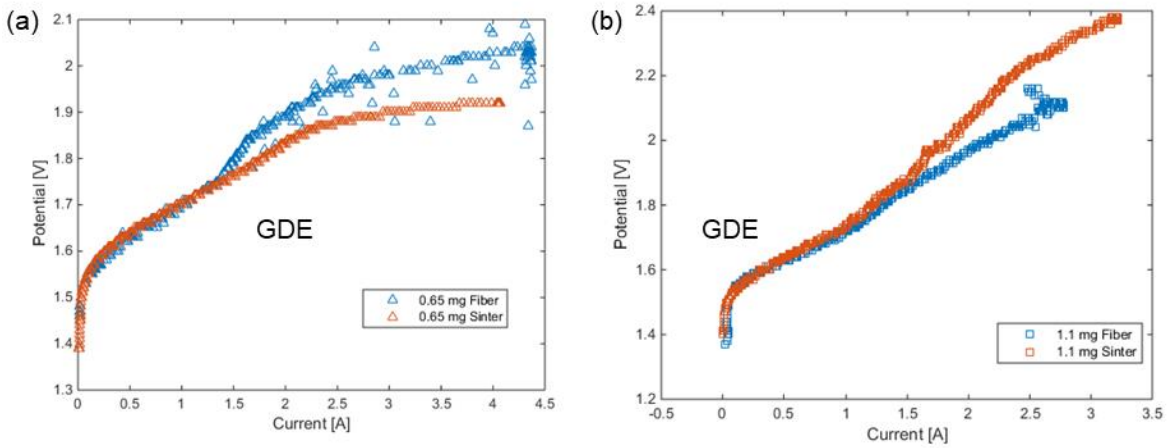

Figure 10. Polarization curves from ALS beamtime comparing a) 0.05 mg/cm^2 loading of fiber and signer PTEs and b) 1.1 mg/cm^2 loading.

Figure 11 shows polarization curves from APS beamtime comparing various loadings for fiber and sinter PTLs. **Figure 11a** shows that the CCM with 1 mg/cm^2 loading shows lower potential than the CCM with 0.5 mg/cm^2. From **Figure 11b** lowering loading from 3 to 1 mg/cm^2 does not seem to increase potential (reduce performance), however reducing it further to 0.5 mg/cm^2 increases potential from 1.65 to 2 V at 4 A/cm^2. Overall, for CCMs, low loaded anodes with 0.5 mg/cm^2 fit better with fiber PTLs, whereas as observed above, for PTEs sintered PTLs work better for low loaded anodes. This can be explained by the fact that in CCM configuration catalyst is deposited onto a membrane and fiber PTLs are more porous hence allow for better mass transport and improved performance.

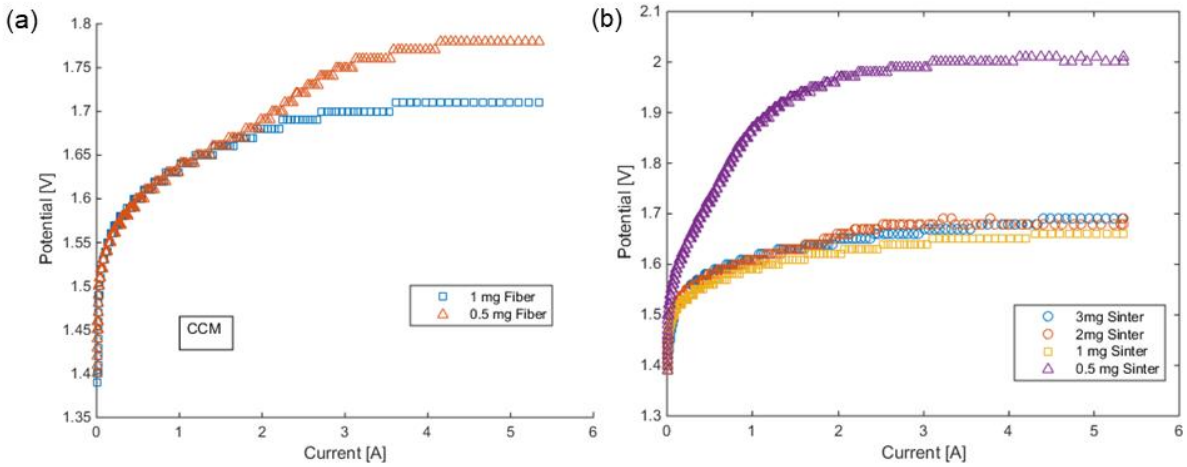

Figure 11. Polarization curves from APS beamtime comparing CCMs at two loadings for a) fiber PTLs and four loadings for b) sinter PTLs.

As a reminder, the following experiments were designed and executed to directly observe water distribution within the PTL. The approach was to simulate PTL morphology but with carbon layer. Since carbon fiber and water attenuation is similar, a machine learning segmentation process was used to distinguish between fiber, water and oxygen. The algorithm involved a student selecting regions of interest and identifying them as “water”, “oxygen” or “solid”. From there the algorithm (Weka, built-in plugin in ImageJ) extrapolated these to a full 2000 images. After review, the algorithm was corrected to ensure that all the oxygen is picked up as oxygen and water as water. UCI also developed a tool to visualize oxygen distribution within the PTL. **Figure 12** shows oxygen concentration thickness for a cell operating at 3 A/cm^2 at three water flowrates. Essentially, all oxygen content is summarized in um of thickness under land and under channel. The highest oxygen content of 165 um is observed under the land location. Overall, the average oxygen content for 3 mlpm slightly decreased compared to 1 and 2 mlpm. These plots indicate that oxygen forms preferential pathways for transport and that the pathways do not change significantly with the change in water flowrate.

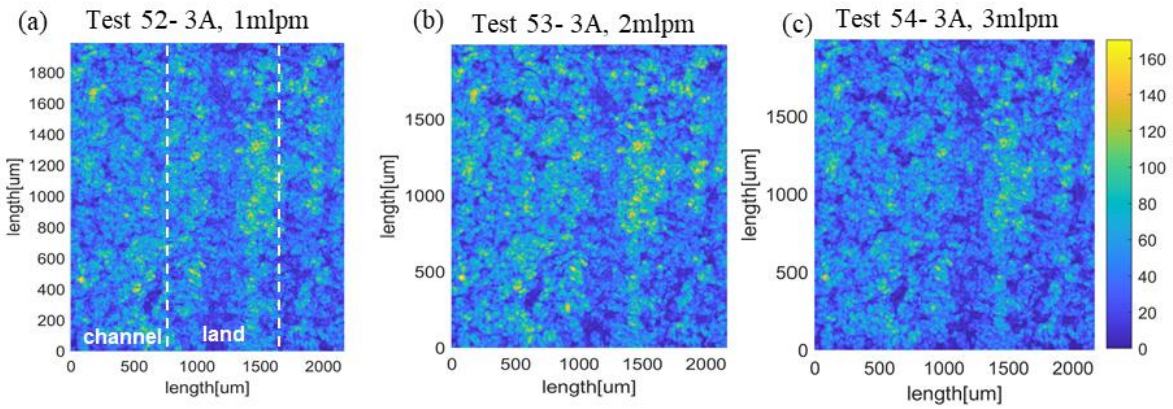

Figure 12. Oxygen concentration under the land and channel for a cell operating at 3 A/cm^2 and flowrates of a) 1 mlpm, b) 2 mlpm and c) 3 mlpm.

Figure 13 shows oxygen distribution under land and channel for electrolyzer operating at the same flowrate but four different current densities. Similar to the results in **Figure 12**, we don't see significant current-density dependence on the water flowrate. Peak oxygen concentration shows under the land in the same location as was shown in **Figure 12**.

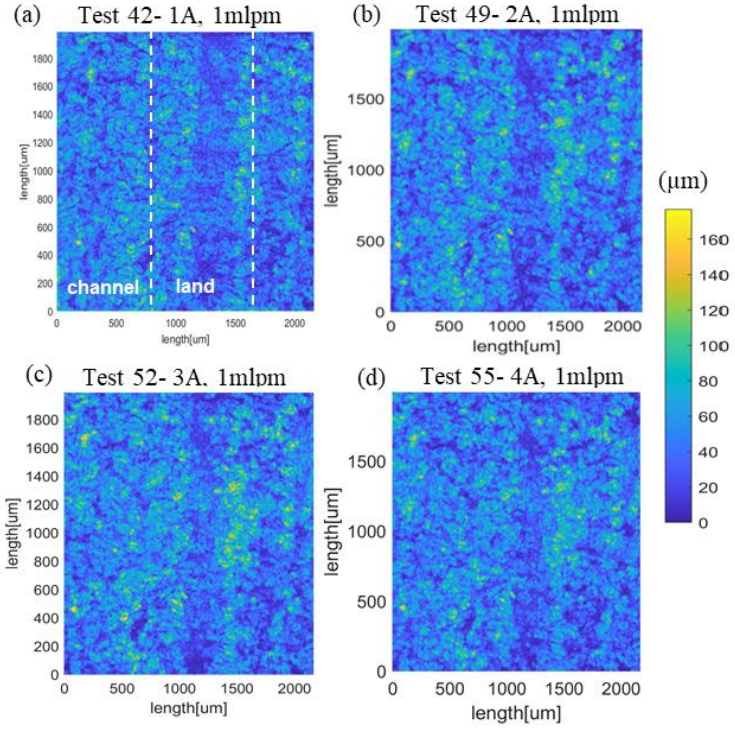

Figure 13. Oxygen concentration under the land and channel for a cell operating at 1 mlpm (low flowrate) and at four different current densities: a) 1 A/cm^2, b) 2 A/cm^2, c) 3 A/cm^2 and d) 4 A/cm^2.

The manuscript based on the above work has been published along with modeling studies, showing that a primary reason for performance loss is low connectivity of catalyst particles with the membrane. Fiber PTLs showed higher porosity and lower tortuosities, but did not necessarily translate into significantly lower potentials.[1]

[1] doi.org/10.1039/C9SE00364A

University of California Irvine (UCI) continued to explore the following tasks: a) Prepared and performed new experiments at the Advanced Light Source (ALS), where cells were reimaged, b) test a new flow-field design to see how it will affect oxygen concentration in the channel, c) begin analyzing all the data for all the porous transport layer (PTL), catalyst coated membrane (CCM) and gas diffusion electrode (GDE) configurations, including radiography, tomography and interface quantification.

a) New experiments were prepared and conducted at the Advanced Light Source (ALS). This time UCI pre-built 4 micro-CT electrolyzers, as reported in **Table 5**, so cells can be preconditioned at UCI to remove in typical break-in prior to testing and verify operability. Some of the cells evaluated were previously imaged cells that were being re-imaged due to issues with the prior test. Cell 3 and Cell 4 had new flow-fields and PTLs from Prof. Feng's group from UTK.

Table 5. Cells tested at ALS beamtime in March 2020

Cell #	**Cell PTL**	**CCM/GDE Loading**
Cell1	CCM	2 mg/cm^2 (CCM)
Cell 2	GDE (sintered)	1.75 mg/cm^2(GDE)
Cell 3	PTL (new flow-field)	3 mg/cm^2(CCM)
Cell 4	Tennessee PTL	3 mg/cm^2(CCM)

Additionally, analysis was performed for the interfaces of operando cells, combining data from all the beamtimes to compare cells operated and imaged for both CCMs and porous transport electrodes (PTEs), where the catalyst loading was varied to look for trends in utilization, depending on the PTL interface. Focus then changed to primarily getting all the reconstructions, interface, and oxygen analysis completed from the radiography data. **Figure 14** shows an interface between one of the PTEs and the membrane interface at three IrOx loadings. The increase in loading can be seen by a corresponding increase in brightness as IrOx content in the electrode goes from 0.65 to 1.75 mg/cm^2. **Figure15** shows the cross-section of these PTE samples at three different loadings. The bright clusters that are observed are the PTE|PEM interface for 1.75 mg/cm^2 of IrOx electrocatalyst.

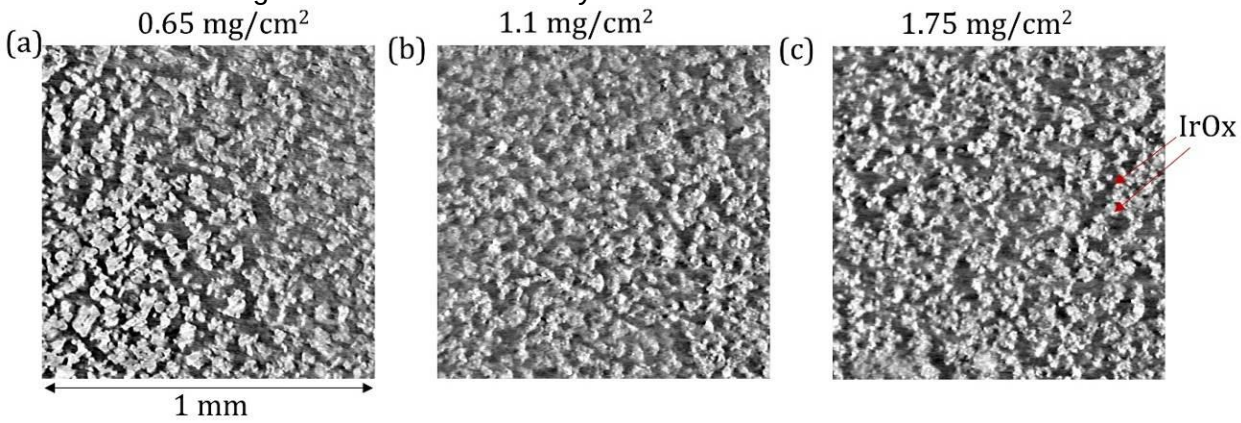

Figure 14. In-plane tomographs. Comparison of sintered PTE|PEM interface for three IrOx loadings on PTEs of a) 0.65 mg/cm^2, b) 1.1 mg/cm^2 and c) 1.75 mg/cm^2.

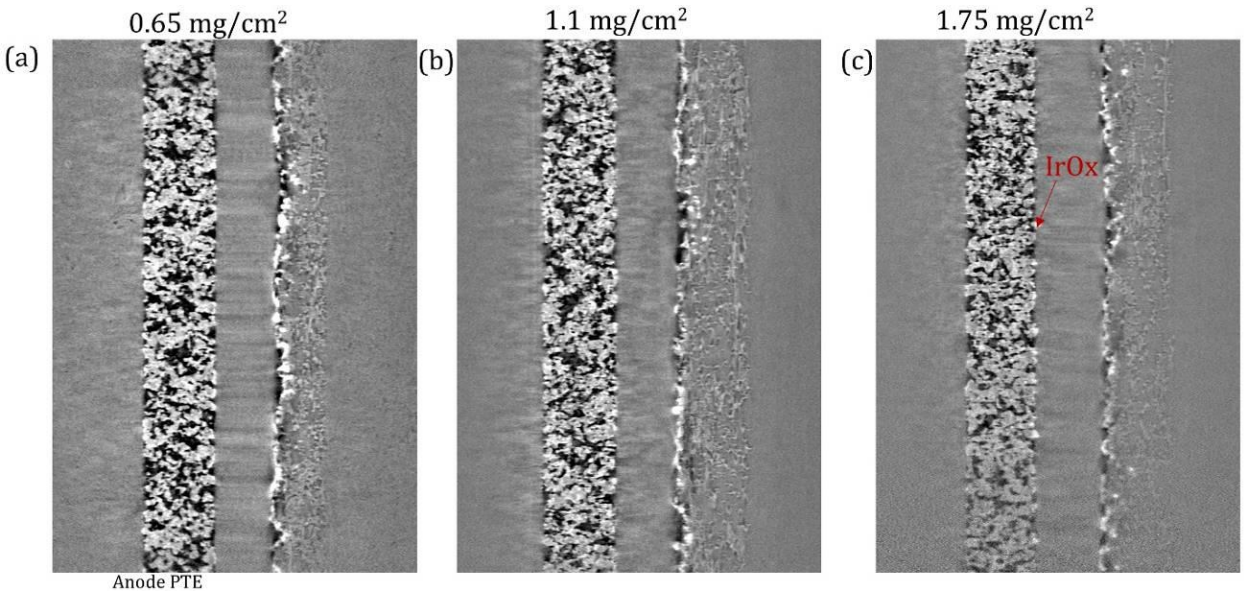

Figure 15. Cross-section x-ray tomographs for PEME with sinter PTEs for three IrOx loadings on PTEs of a) 0.65 mg/cm^2, b) 1.1 mg/cm^2 and c) 1.75 mg/cm^2.

Figure 16 shows an in-plane tomograph of the fiber PTE|PEM interface for three IrOx loadings of 0.65, 1.1 and 1.75 mg/cm^2. IrOx is clearly deposited only onto the fibers and with increase in loadings show a higher degree of agglomeration. The loadings difference between these three samples is more pronounced for fiber PTE, as compared to sinter PTE. **Figure 17** shows the cross-sections for PEME with fiber PTEs. Again, brighter IrOx is observed at the higher loading of 1.75 mg/cm^2 compared to that at 0.65 mg/cm^2.

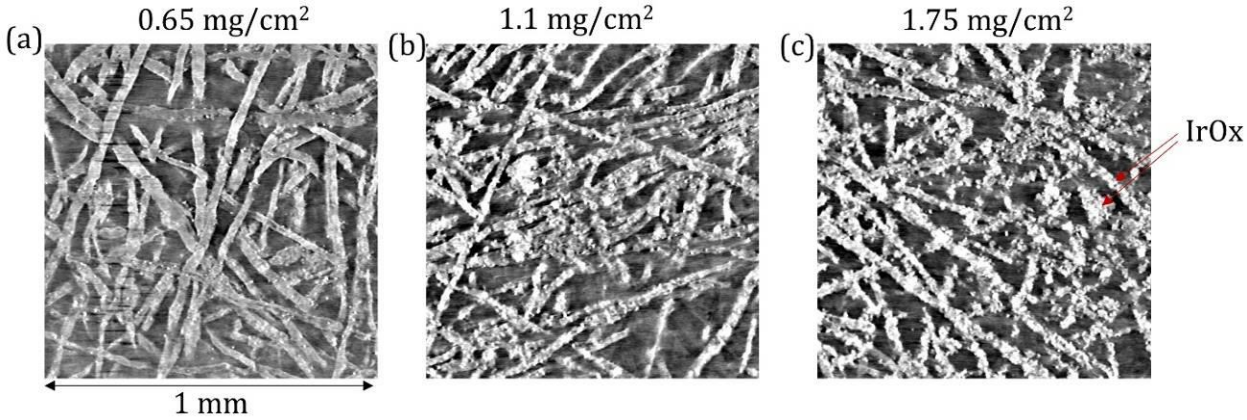

Figure 16. In-plane tomographs. Comparison of fiber PTE|PEM interface for three IrOx loadings on PTEs of a) 0.65 mg/cm^2, b) 1.1 mg/cm^2 and c) 1.75 mg/cm^2.

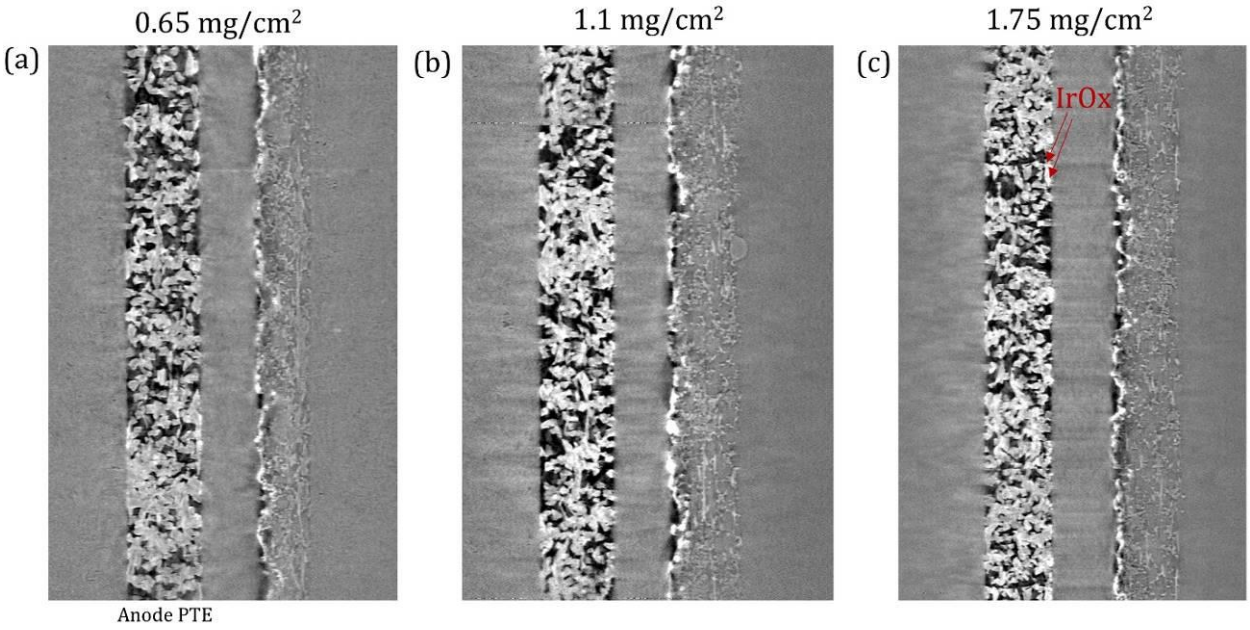

Figure 17. Cross-section x-ray tomographs for PEME with fiber PTEs for three IrOx loadings on PTEs of a) 0.65 mg/cm^2, b) 1.1 mg/cm^2 and c) 1.75 mg/cm^2.

Work at the end of the project focused on analyzing oxygen content in the channels for the PEME cell with these various CCM/PTL configurations was also conducted using x-ray radiography. **Figure 18a** shows oxygen percent in the channel as a function of current density for the CCM with 1 mg/cm^2 This CCM was evaluated with interfaces comprised of both sinter and fiber PTLs. As current density increases from 1 to 5 A/cm^2, oxygen content in the channel increases from 40% to 70%. Both sintered and fiber PTLs show very similar oxygen content in the channel indicating that their mass transport is quite similar. **Figure 18b** shows oxygen percent in the channel through a range of current densities for a CCM with a loading of 0.5 mg/cm^2. Sinter PTLs show oxygen content flattening out after 3 A/cm^2, whereas fiber PTLs show increasing oxygen content in the channel, as current density increases from 1 to 4 A/cm^2. It is believed that having higher oxygen content in the channel is desirable, as it shows that the PTL can remove oxygen effectively from the electrode surface.

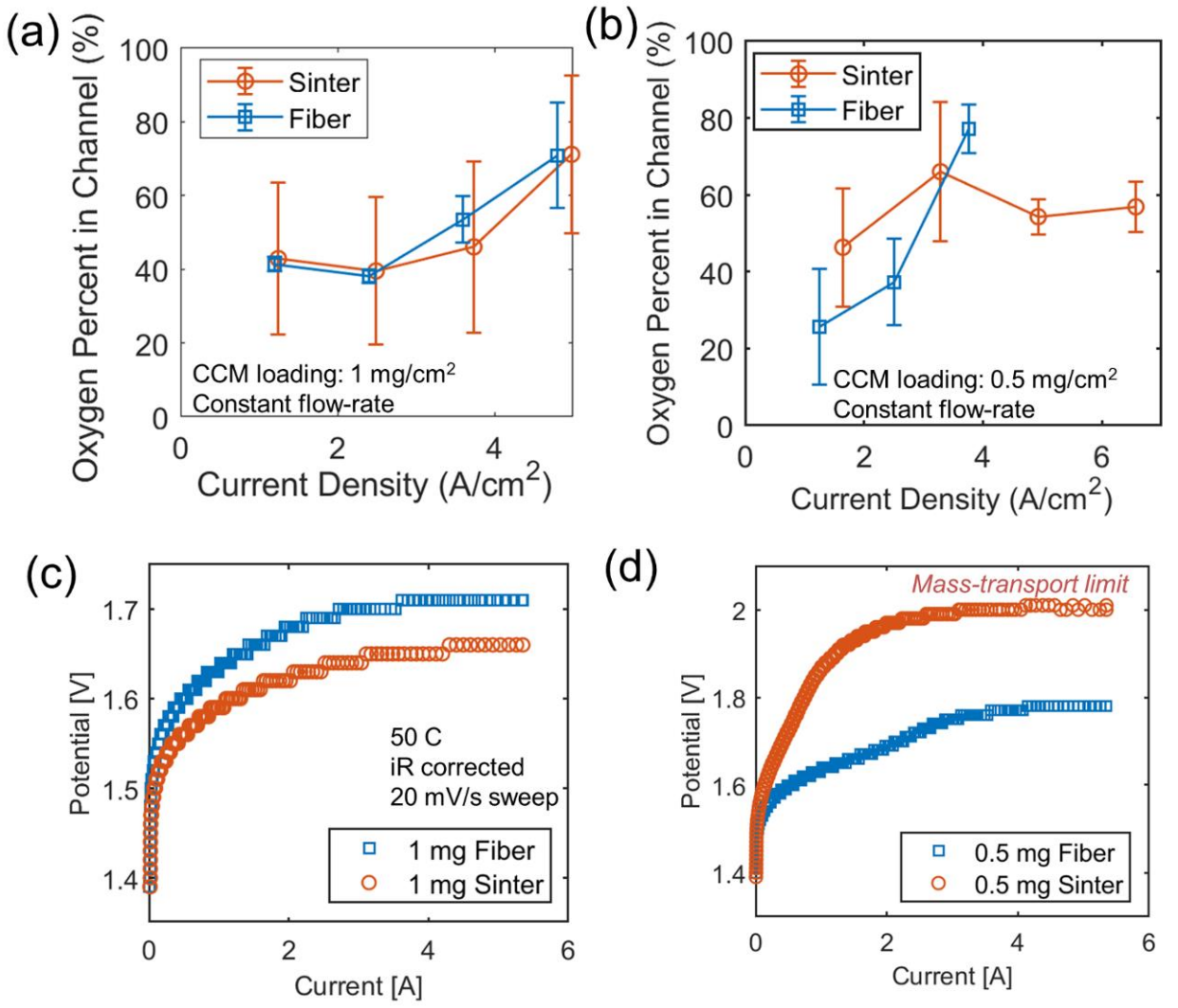

Figure 18. a) Oxygen percent in channel as a function of current density for CCM with loading of 1 mg/cm^2 comparing sinter and fiber PTLs. b) oxygen percent in channel as a function of current density for CCM with loading of 0.5 mg/cm^2 comparing sinter and fiber PTLs. c) Polarization curves from x-ray CT operando cell comparing 1 mg CCM with fiber and sintered Ti. d) 0.5 mg CCM with fiber and sinter PTLs.

Figure 18c and d show polarization curves from the 1 cm^2 active area electrolyzer from the beamtime. Both PTLs show similar polarization behavior for CCMs with 1 mg/cm^2 IrOx electrocatalyst, whereas CCMs with 0.5 mg/cm^2 fiber PTL showed better polarization behavior than 0.5 mg/cm^2 sintered PTL. We also observe that sintered PTL had lower oxygen content in the channel; as already indicated, lower oxygen content should translate to worse performance as it is indicative of the cell's challenge to remove oxygen from the electrode.

University of California Irvine (UCI) the change focus onto the following tasks: a) Finish analyzing data for radiography, tomography, interface quantification and oxygen content correlation to potential, b) Complete the manuscript for 3D Lattice-Boltzmann simulations to explain oxygen distribution in the PTLs, c) Completed manuscript summarizing different PTE vs CCM loading and interfacial analysis.

We also completed analysis of data from the four beamtimes and organized it by PTL type and loading as shown by **Table 5**. The tested samples over the last year were either CCMs or PTEs. The types of PTLs were either fiber or sinter PTLs. The IrOx loading varied from 0.5 to 2 mg/cm^2, as shown by **Table 5**. Two of the cells had issues, with polarization curve data showing higher voltages than expected.

Cell #	**Cell Type**	**Loading**
Cell 6, Nov 2019	CCM, Fiber PTL	0.5 mg/cm^2
Cell 2, Nov 2019	CCM, Fiber PTL	1 mg/cm^2
Cell 5, Nov 2019	CCM, Fiber PTL	2 mg/cm^2
Cell 1, Nov 2019	CCM, Sinter PTL	0.5 mg/cm^2
Cell 2, Nov 2019	CCM, Sinter PTL	1 mg/cm^2
Cell 6, Mar 2020	CCM, Sinter PTL	2 mg/cm^2
Cell 1, Oct 2019	PTE, Fiber PTL	0.65 mg/cm^2
Cell N, Oct 2019	PTE, Fiber PTL	1.1 mg/cm^2
Cell 3, Oct 2019	PTE, Fiber PTL	1.75 mg/cm^2
Cell1, Mar 2020	PTE, Fiber PTL	2 mg/cm^2
Cell 4, Oct 2019	PTE, Sinter PTL	0.65 mg/cm^2
Cell M, Oct 2019	PTE, Sinter PTL	1.1 mg/cm^2
Cell 6, Oct 2019	PTE, Sinter PTL	1.75 mg/cm^2

Table 5. Cells used for loading and PTL comparison from October, November 2019 and March 2020 beamtimes. The highlighted cells experienced data processing issues.

In the following section we summarize the x-ray CT results. **Figure 19** shows IrOx distribution at the interface between CCM and PTL that is fibrous. From the images and volume renderings we observed sparse catalyst distribution for the 0.5 mg/cm^2 loaded sample, more uniform electrocatalyst distribution at 1 mg/cm^2 and some evidence of agglomerates forming for the IrOx loading of 2 mg/cm^2. Note that the micro x-ray CT technique is only able to capture domains with resolution of 1.3 um in size or larger. From optical images catalyst is uniformly coated in all three cases. However, its thickness might be on the order of 1 um and hence not captured by micro x-ray CT.

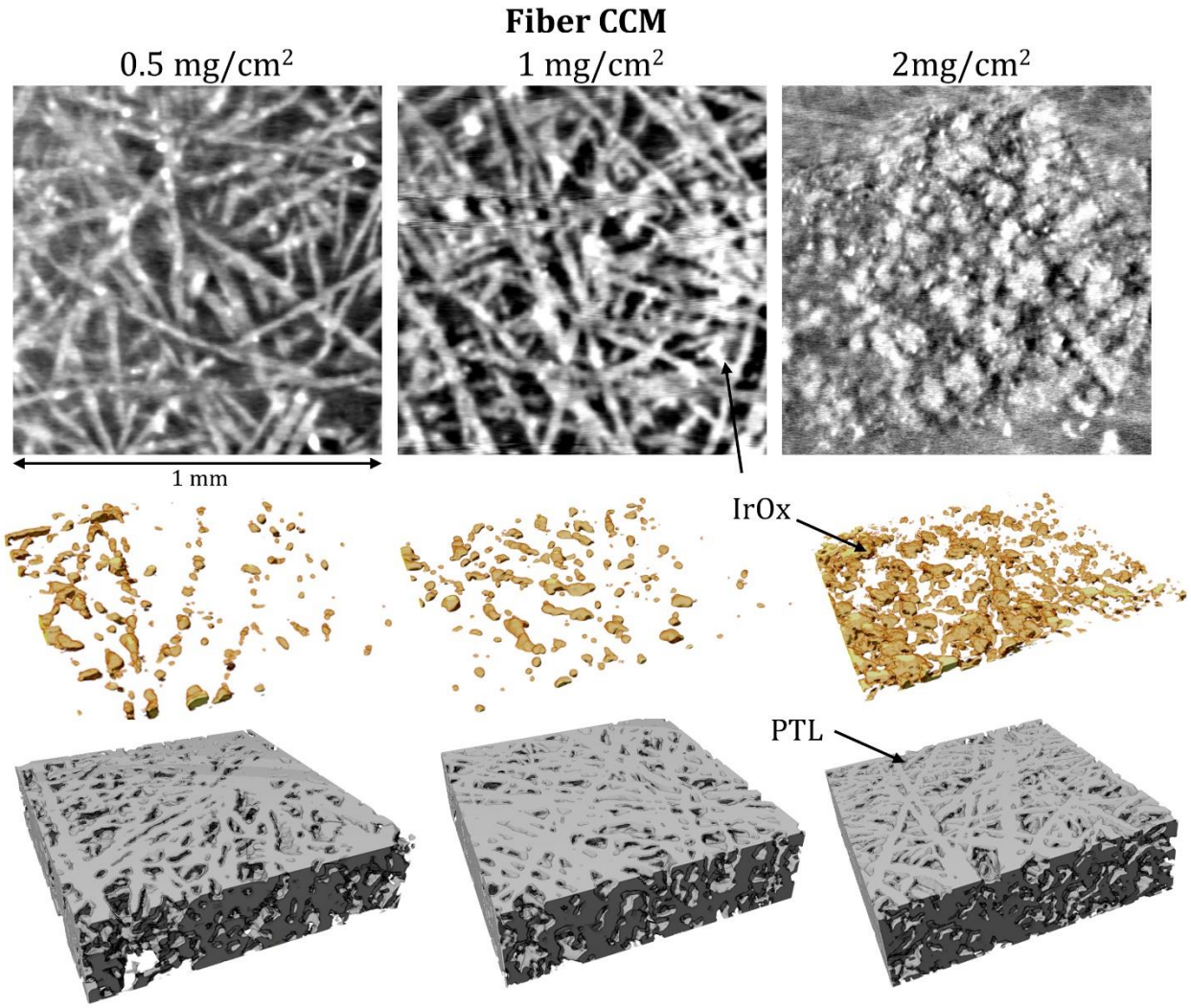

Figure 19. Cross-section x-ray tomographs showing IrOx distribution at the interface between CCM and fiber PTL for 0.5, 1 and 2 mg/cm^2. The second row shows volume rendered catalyst layer and the bottom row shows volume rendered PTL.

Figure 2020 shows the results for the catalyst distribution at the interface of CCMs and sinter PTLs with 0.5 and 2 mg/cm^2. Essentially, these are the same CCMs as used for **Figure 19** but the PTL was exchanged for sintered particles instead of fiber. Similar catalyst distribution was observed in both cases.

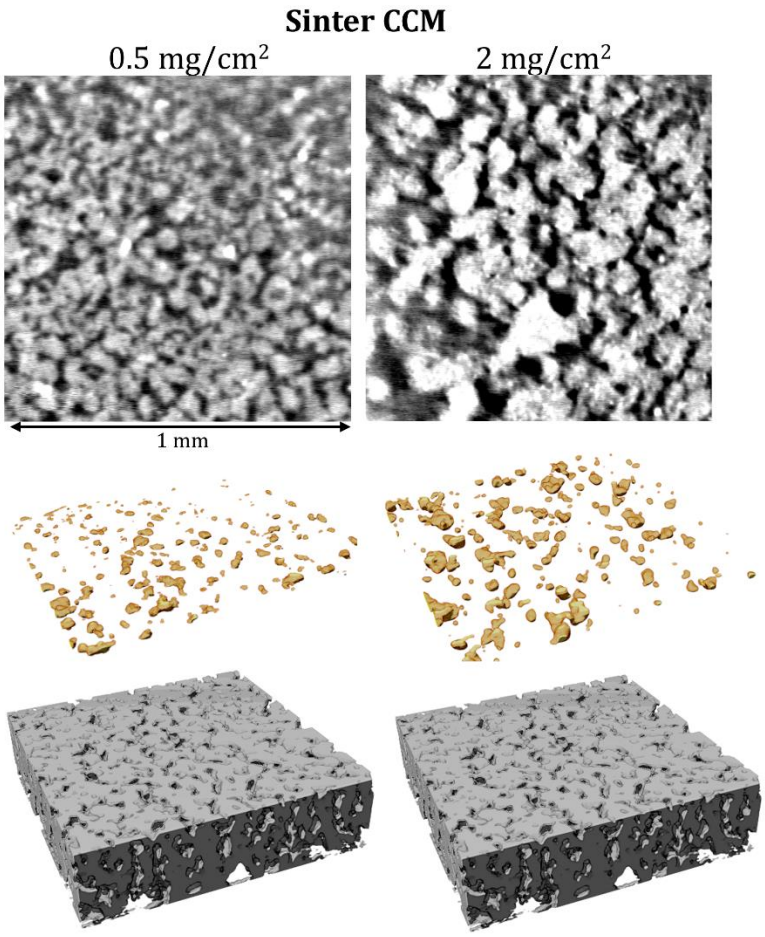

Figure 20. Cross-section x-ray tomographs showing IrOx distribution at the interface between CCM and sintered PTL for 0.5 and 2 mg/cm^2. The second row shows volume rendered catalyst layer and the bottom row shows volume rendered PTL.

Figure 2121 shows the interface for PTE and membrane and associated electrocatalyst distribution for 0.65, 1.1 and 1.75 mg/cm^2 loadings for fibrous PTLs. In contrast to CCMs, these fibrous PTEs show catalyst distribution that is on top of fibrous region only. The catalyst distribution and volume increase from 0.65 to 1.75 mg/cm^2 as evident from **Figure 2121**. No significant agglomeration was observed for these PTEs.

Figure 22 shows sintered PTLs coated with IrOx for the same loadings as those in **Figure 2120**, where volume rendered catalyst layers are also shown. Catalyst volume did not appear to increase with a loading increase from 0.65 to 1.1 mg/cm^2. Dense coatings were observed for the sample with 1.75 mg/cm^2 loading.

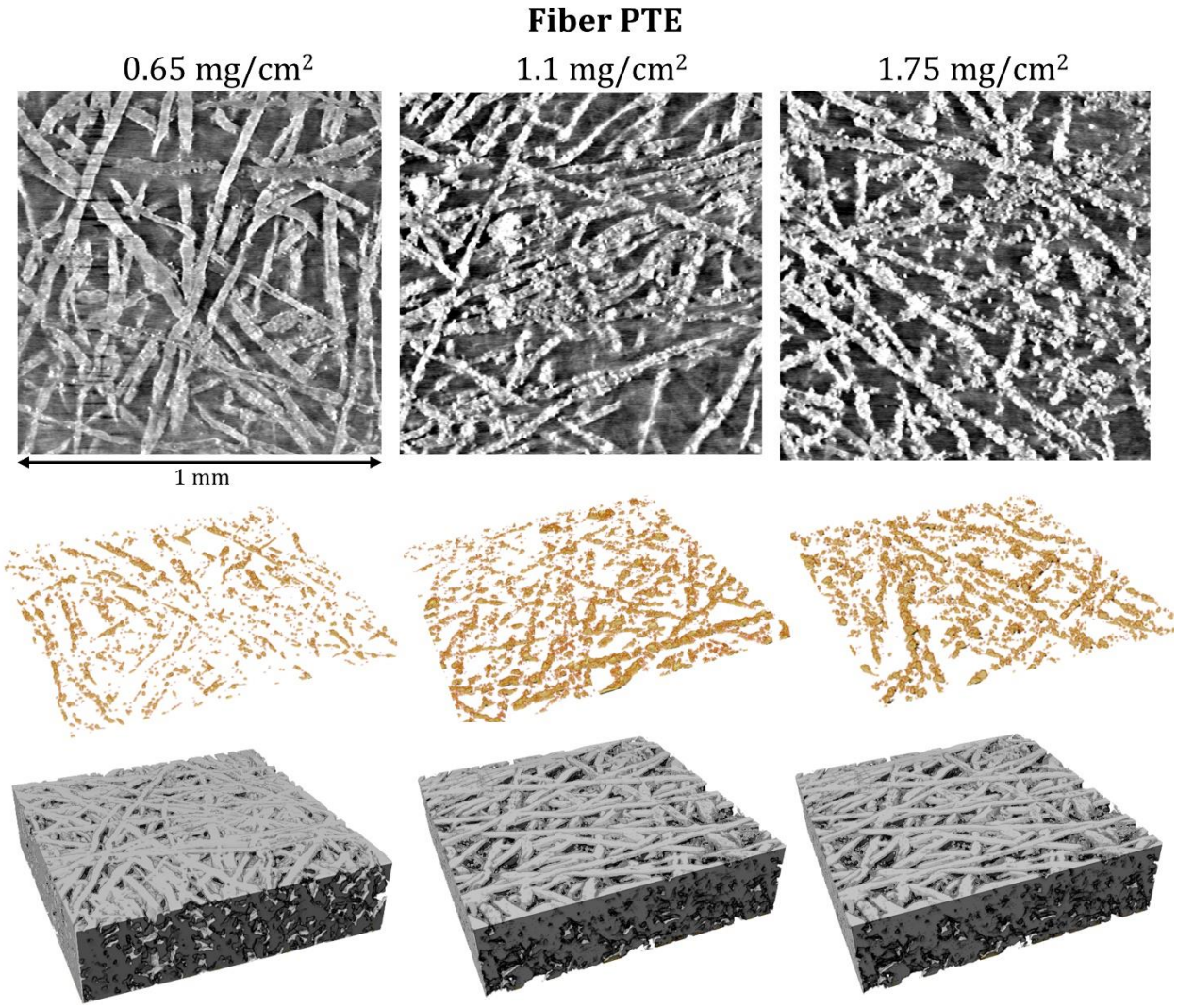

Figure 21. Cross-section x-ray tomographs showing IrOx distribution at the interface between fiber PTE and membrane for 0.65, 1.1 and 1.75 mg/cm^2. The second row shows volume rendered catalyst layer and the bottom row shows volume rendered PTLs.

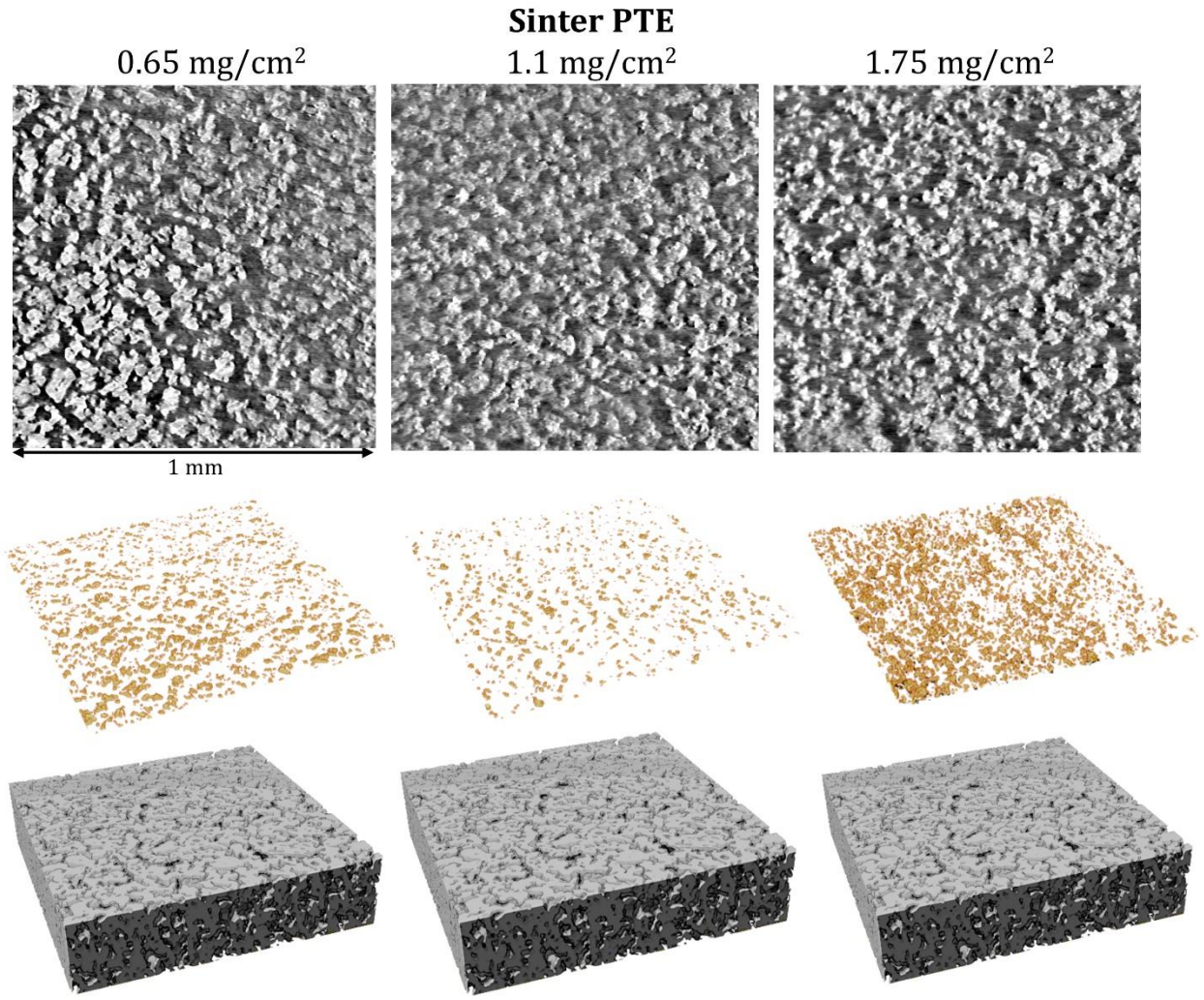

Figure 22. Cross-section x-ray tomographs showing IrOx distribution at the interface between sintered PTE and membrane for 0.65, 1.1 and 1.75 mg/cm^2. The second row shows volume rendered catalyst layer and the bottom row shows volume rendered PTLs.

Figure 23 shows oxygen content in the channel for a range of current densities from 1 A/cm^2 to 6 A/cm^2 vs. voltage of the cell. Oxygen concentration increases as current density increases, starting from about 40 % in the channel for higher loading and 1 A/cm^2 and 25 % for low loaded catalyst. Higher oxygen content in the channel is due to larger oxygen bubbles and slugs forming as oxygen transports through the PTL and is getting ejected into the channel. Oxygen content increases to 60 % for higher loaded CCMs at 5 A/cm^2 and to a higher value of 80 % for the lowest loaded catalyst layer. The oxygen content and potential data are available for all the other PTEs and CCMs, but representative examples are shown to save space.

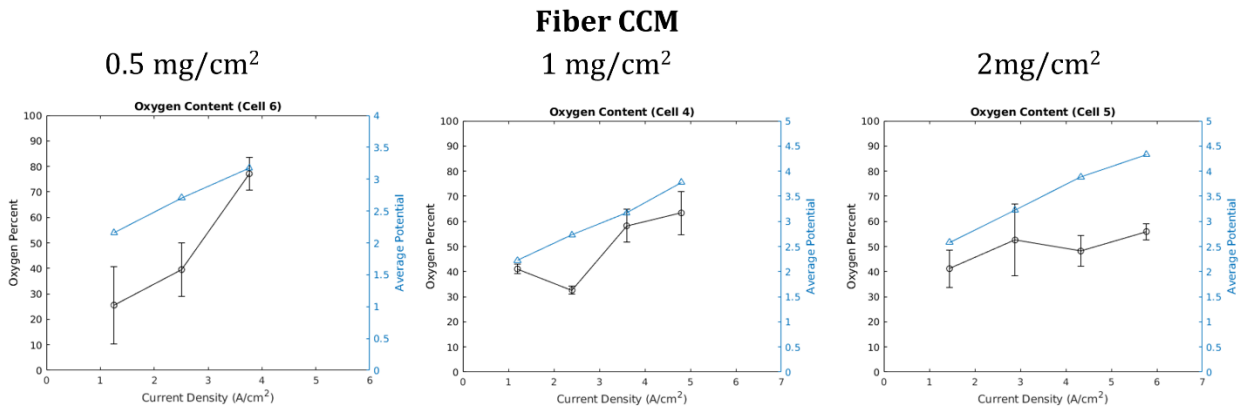

Figure 23. Oxygen content in the channel with x-ray radiography, as a function of current density for fiber PTL CCM configuration. The CCM loadings are 0.5, 1 and 2 mg/cm^2. Average potential is plotted on the right y-axis.

Figure 24 shows percentage of contact area of catalyst between PTL and membrane. Figure 8a shows comparison between CCMs in contact with fiber and sinter PTLs, with 2 mg/cm^2 loading. Sintered PTLs generally have lower porosity than fiber PTLs and also show higher contact area at 60 % compared to 42 % for sintered PTLs. **Figure 24b** shows interfacial contact area for 0.5 mg/cm^2 catalyst loading, which shows 4-6 times lower contact area than 2 mg/cm^2 loading, at around 10%. Increasing the loading 4 times translates in similar amount of contact area increase. Lastly, Figure c compares CCMs and fiber PTEs of three similar loadings. The contact area increased from around 10 % for 0.5 or 0.65 mg/cm^2, to 20 % for 1 and 1.1 mg/cm^2, to 40-50 % for 1.75 and 2 mg/cm^2.

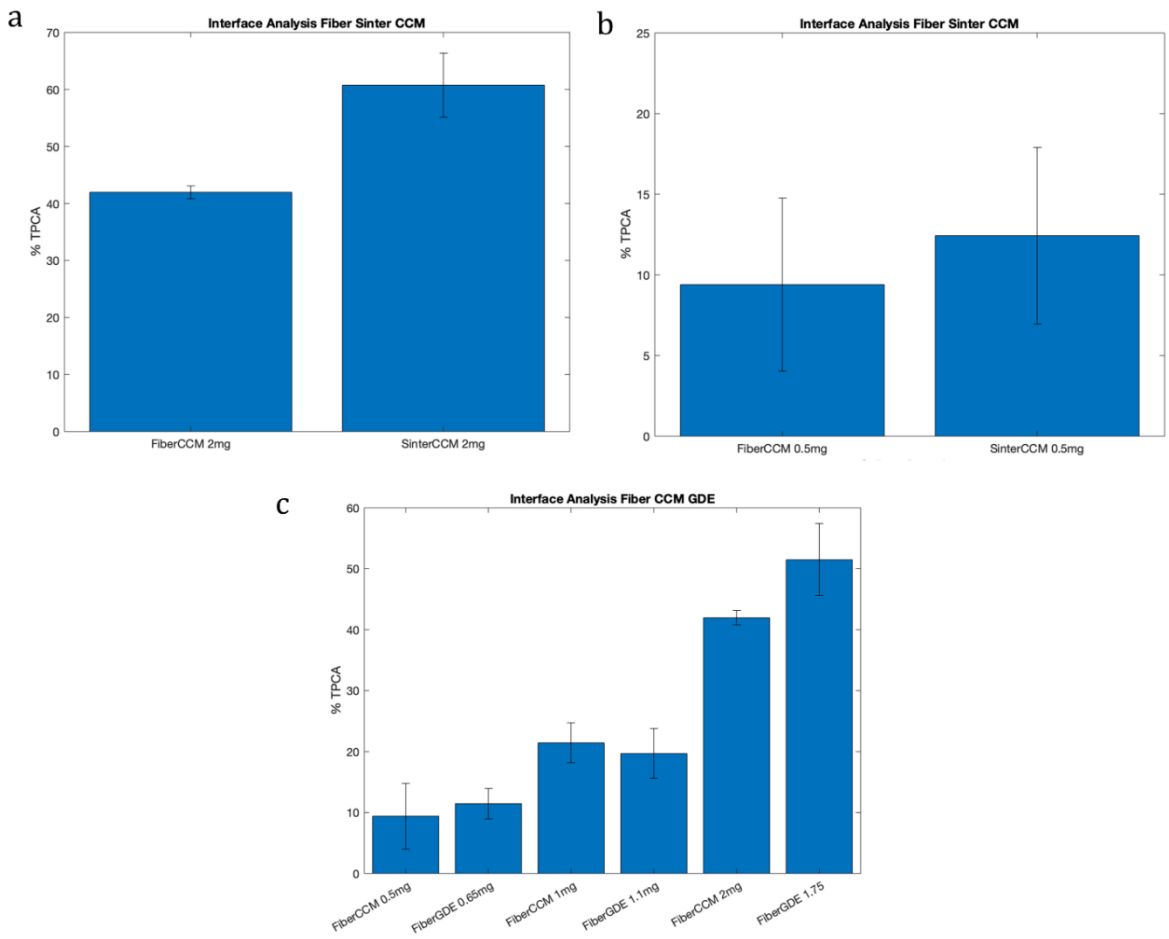

Figure 24. Percentage of contact area comparing a) fiber and sinter PTLs with CCM loaded with 2 mg/cm^2 IrOx, b) fiber and sinter PTLs with CCM loaded with 0.5 mg/cm^2 and c) fiber PTLs and PTEs with CCMs having various loading.

Figure 2525 shows the oxygen distribution within the PTL, where focus is on three locations: near the catalyst layer, in the middle of the PTL, and at the interface with the channels and land. Oxygen content decreases from 0.4 volume fraction near the catalyst layer to 0.05 near the flow-field. This figure shows the results for 1 A/cm^2 current density. **Figure 2525c-e** show in-plane oxygen content in these three locations. We observe a periodic waveform of oxygen content in the PTL with the periodicity of 400 um.

Figure 2626 shows the same plots but for 4 A/cm^2 current density. Oxygen content didn't change with current density, as oxygen is preferentially removed through the same pathways. At 4 A/cm^2 we observe higher oxygen concentration under the land at the catalyst interface with the PTL.

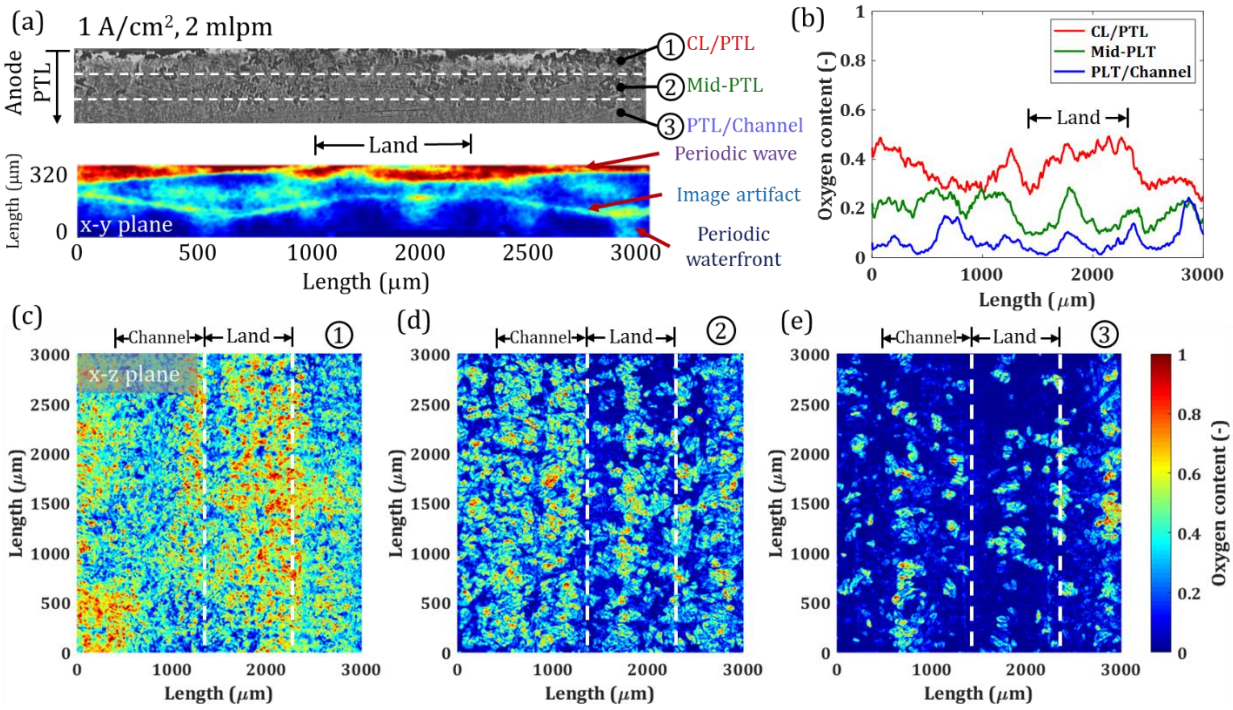

Figure 25. The comparison of oxygen content within the different portions of PTL at the operating condition of 1 A/cm^2, 2 mlpm. (a) (Top) 1/3 portions of PTL representing CL/PTL interface, Middle of PTL, and PTL/channel interface. (Bottom) 2D oxygen content of PTL at x-y plane by using Z-project method. (b) Oxygen content comparison at different PTL portions. (c) Z-project of the oxygen content of the x-z plane at the CL and PTL interface. (d) Z-project of the oxygen content of the x-z plane at the middle PTL portion. (e) Z-project of the oxygen content of the x-z plane at the PTL and channel interface.

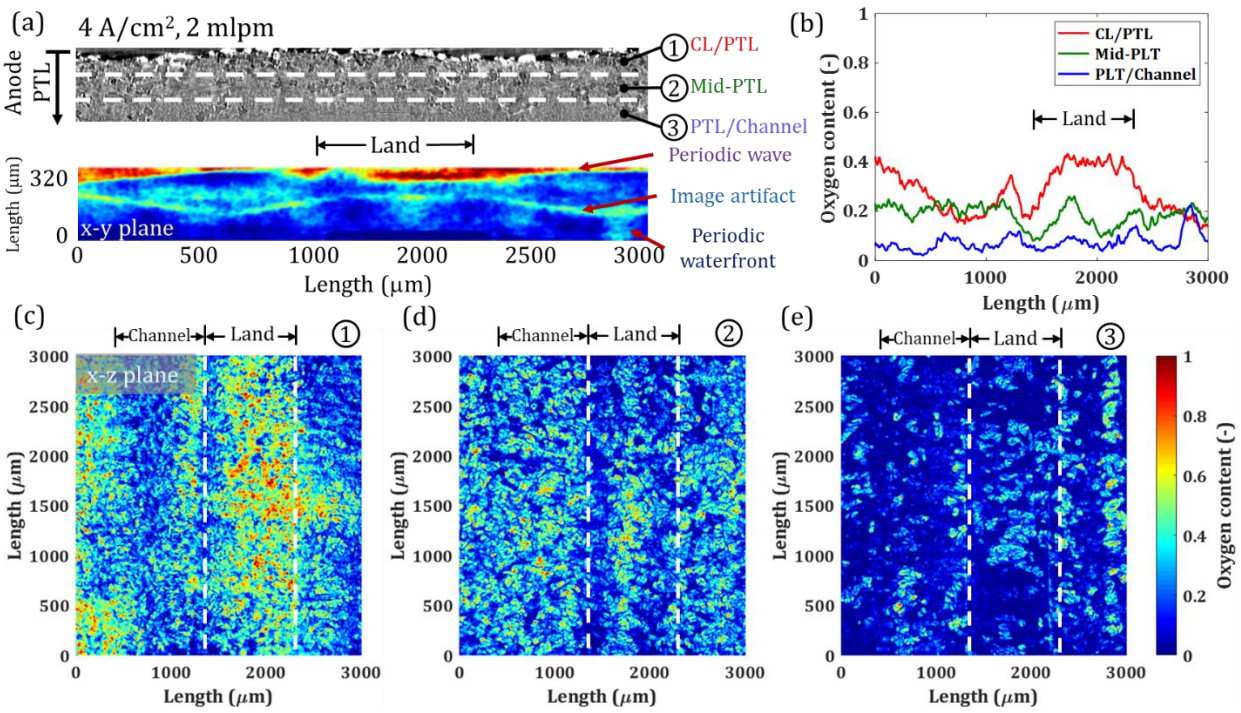

Figure 26. The comparison of oxygen content within the different portions of PTL at the operating condition of 4 A/cm^2, 2 mlpm. (a) (Top) 1/3 portions of PTL representing CL/PTL interface, Middle of PTL, and PTL/channel interface. (Bottom) 2D oxygen content of PTL at x-y plane by using Z-project method. (b) Oxygen content comparison at different PTL portions. (c) Z-project of the oxygen content of the x-z plane at the CL and PTL interface. (d) Z-project of the oxygen content of the x-z plane at the middle PTL portion. (e) Z-project of the oxygen content of the x-z plane at the PTL and channel interface.

A 3D Lattice-Boltzmann model was also developed to simulate oxygen content in the PTLs. The comparison between the experiment and modeling data is shown by **Figure 2727**, where average concentrations show very good agreement. The model predicts oxygen removal from selected locations that were 400 um apart.

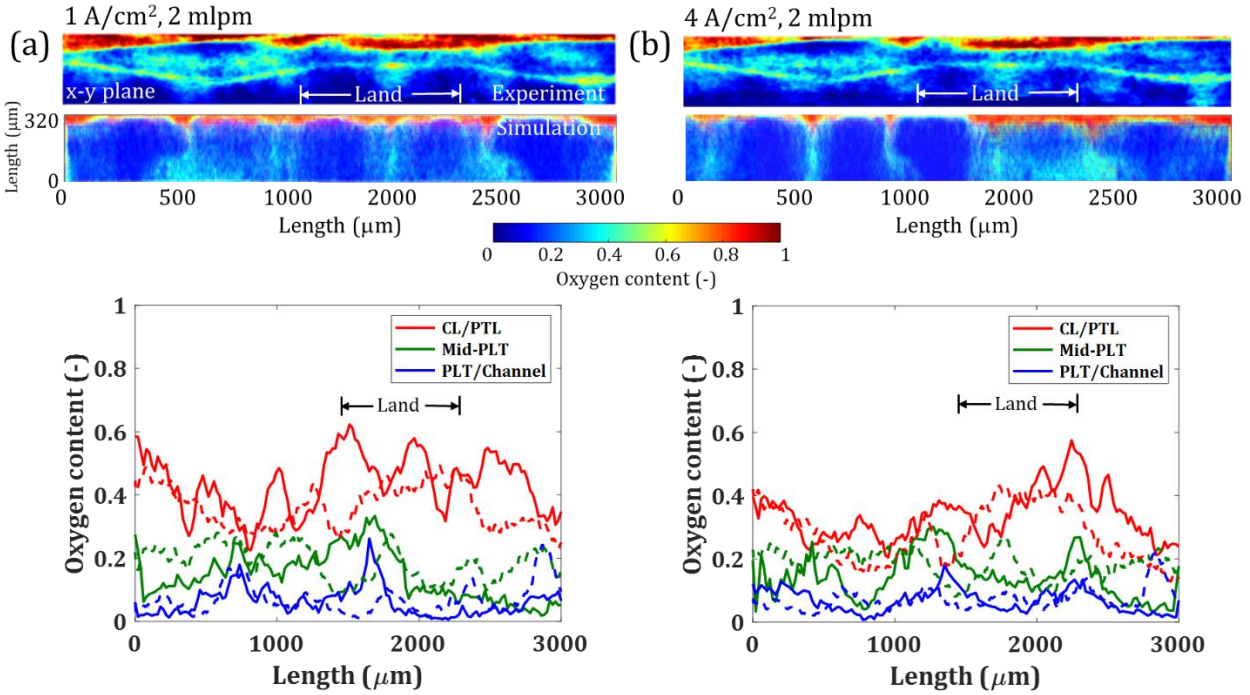

Figure 27. Dashed line (--): experiment, Solid line (–): modeling. (a) CFD simulation comparison with experimental results at the operating condition of 1 A/cm^2, 2 mlpm. (b) CFD simulation comparison with experimental results at the operating condition of 4 A/cm^2, 2 mlpm.

Task 3: Advanced Catalyst

Key Findings: Advanced Catalyst

- The blended catalysts all performed relatively well, except for the catalyst with high niobium content, indicating the non-active material dominated the catalyst properties.
- Higher metal and ruthenium content resulted in higher dissolution rates and activity loss.
    - Conversely, minimal activity loss was seen for catalysts that contained only Ir or ruthenium-containing catalysts that were primarily oxides

Catalyst electrochemical surface areas (ECAs) were determined through mercury underpotential deposition and confirmed with Brunauer–Emmett–Teller (BET) measurements. ECA determinations leverage previous efforts determining the surface areas of iridium (Ir) and Ir oxide nanoparticles. [2]While the use of mercury underpotential deposition aids in ECA measurements in this study, it also tests the robustness of the method by incorporating different material sets that contain ruthenium and a wider variety of surface areas. Surface areas determined by mercury underpotential deposition (**Figure 28**, green) and BET (**Figure 28,** yellow) were generally similar across material types and synthesis approaches. Deviations, however, were found in instances where the BET surface area was very high, in excess of 100 m^2 g^{-1}. ECA measurements for these materials may therefore require a lower loading in rotating disk electrodes to properly capture high ECAs and fully utilize available surfaces. Mercury underpotential deposition, however, may struggle to access sites electrochemically when the bulk catalyst size is large and highly porous, depending on the pore size.

[2] S.M. Alia, K.E. Hurst, S.S. Kocha, B.S. Pivovar, *J. Electrochem. Soc.*, **2016**, 163(11), F3051.

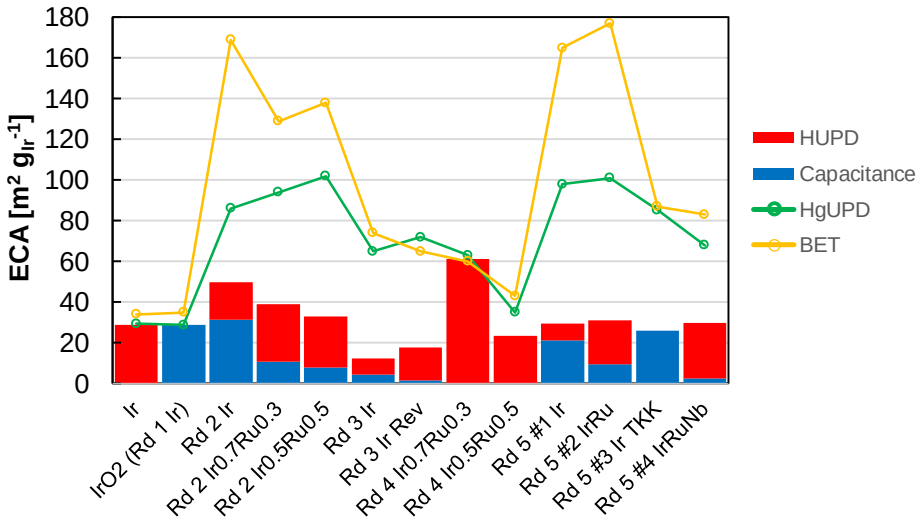

Figure 28. ECAs of screened catalysts, including the responses from hydrogen underpotential deposition (HUPD, red), capacitance (blue), mercury underpotential deposition (HgUPD, green), and BET (yellow).

Additionally, catalysts were evaluated with hydrogen underpotential deposition and capacitance measurements to approximate surface contributions from metals and oxides (**Figures 28 and 29**). These types of determinations are useful to understanding membrane electrode assembly performance and durability, where metals tend to show higher activity in rotating disk electrodes but have a higher dissolution rate. [3]While hydrogen underpotential deposition is relatively straightforward, using capacitance to estimate oxide content is inherently complicated since capacitance is a bulk measurement and not surface sensitive. It is useful, however, as a qualitative comparison. When comparing the screened catalysts, there were two instances where the catalysts gave large hydrogen underpotential deposition responses and ECAs (from HUPD) that were comparable to mercury underpotential deposition, indicating that the catalyst was primarily metallic. Conversely, there was one catalyst that gave a large capacitance and an ECA (from capacitance) that was comparable to mercury underpotential deposition, indicating that the catalyst was primarily an oxide. For the majority of materials, however, the ECAs (HUPD and capacitance) did not reach that of the mercury underpotential deposition. This indicated that the catalyst was a mixed oxide, where the catalyst surface was not entirely metallic (to increase the HUPD response) and not an oxide throughout (to increase the capacitance).

[3] S.M. Alia, M.-A. Ha, G.C. Anderson, C. Ngo, S. Pylypenko, R.E. Larsen, *J. Electrochem. Soc.*, **2019**, *166*(15), F1243.

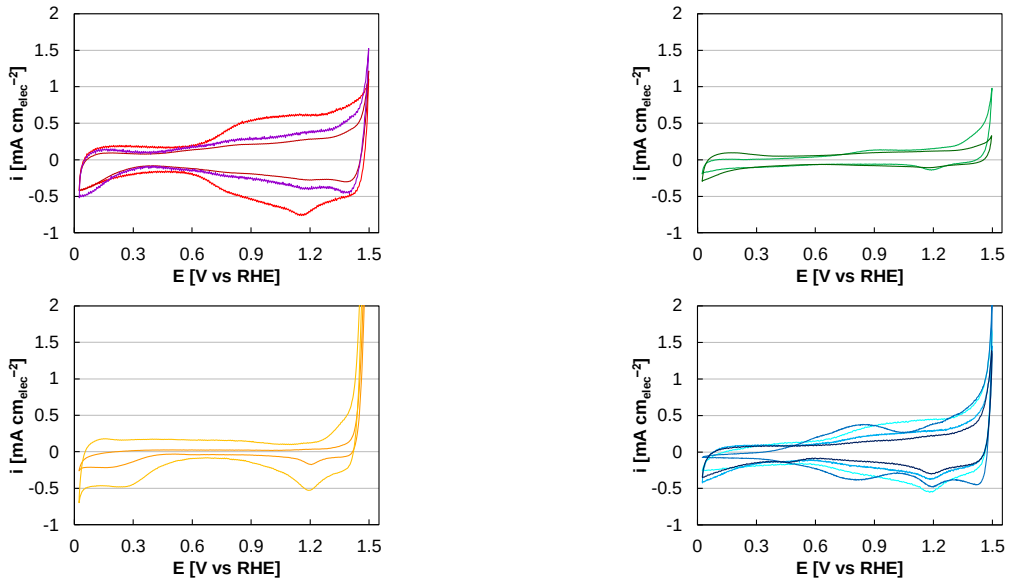

Figure 29. Cyclic voltammograms of catalysts, used to determine ECA for hydrogen underpotential deposition and capacitance. Catalysts were separated based on being screened in Round 2 (reds), 3 (greens), 4 (yellows), and 5 (blues).

Catalysts were further examined with scanning electron microscopy (SEM) and x-ray diffraction (XRD). While none of the catalysts were particularly ordered or clearly faceted, SEM showed differences in particle size and porosity, where some of the catalysts fragmented into small particles and others aggregated but had rough, porous surfaces (**Figure 30**). While large degrees of alloying were not found, XRD demonstrated a range in crystallinity and included several catalysts that were highly crystalline (**Figure 31**).

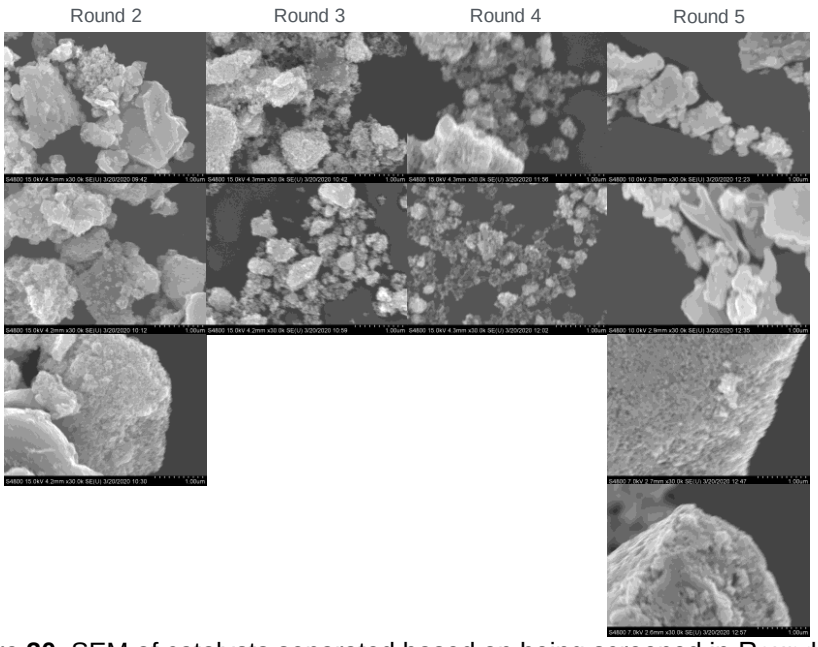

Figure 30. SEM of catalysts separated based on being screened in Round 2–5.

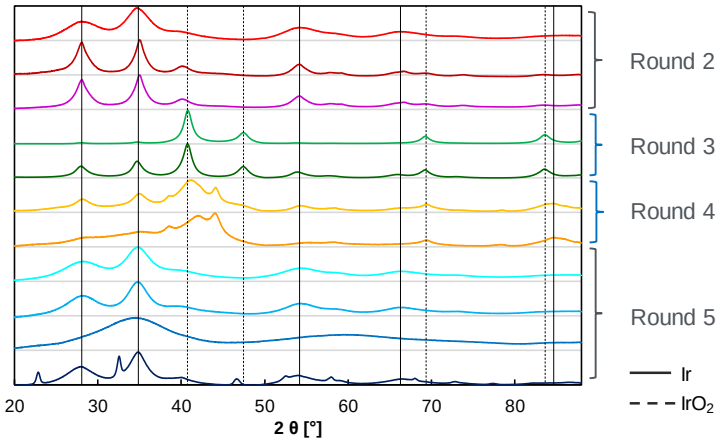

Figure 31. XRD of catalysts, separated based on being screened in Round 2–5. Reference peak locations were included for Ir (solid) and Ir oxide (dashed).

Mercury underpotential deposition measurements were used to determine site-specific OER activity (**Figure 32**). In general, and as expected, higher specific activity was found when the catalyst included ruthenium or niobium. Within these subsets, higher metal composition also improved activity, particularly in Round 4 where the specific activities were 2–8 times more active than the other ruthenium-containing catalysts. Beyond these two factors (ruthenium, metal/oxide), however, no clear trend was observed with respect to catalyst morphology or the degree of crystallinity. In rotating disk electrode stability testing, expected results were found (**Figure 33**). Higher metal and ruthenium content resulted in higher dissolution rates and activity loss. This was particularly noticeable for the Round 4 catalysts (primarily metal, contained ruthenium), where nearly all activity was lost. Conversely, minimal activity loss was seen for catalysts that contained only Ir or ruthenium-containing catalysts that were primarily oxides (Round 5 #2, #4). In cases, the activity losses were worse than expected from the dissolution data (Round 4). This may be due to relatively fast dissolution rates where catalyst layer delamination occurred that was not detected by inductively coupled plasma-mass spectrometry (ICP-MS). It is possible that the combination of metal surfaces and ruthenium content may exacerbate the issue.

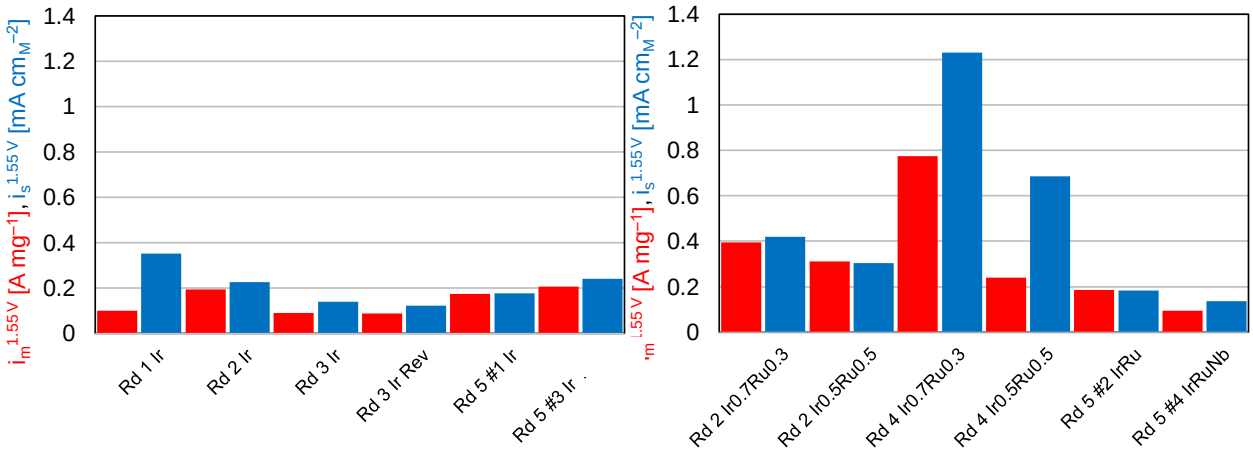

Figure 32. Mass (red) and specific (blue) OER activities of screened catalysts, separated based on materials that (a) contained only Ir or (b) including ruthenium.

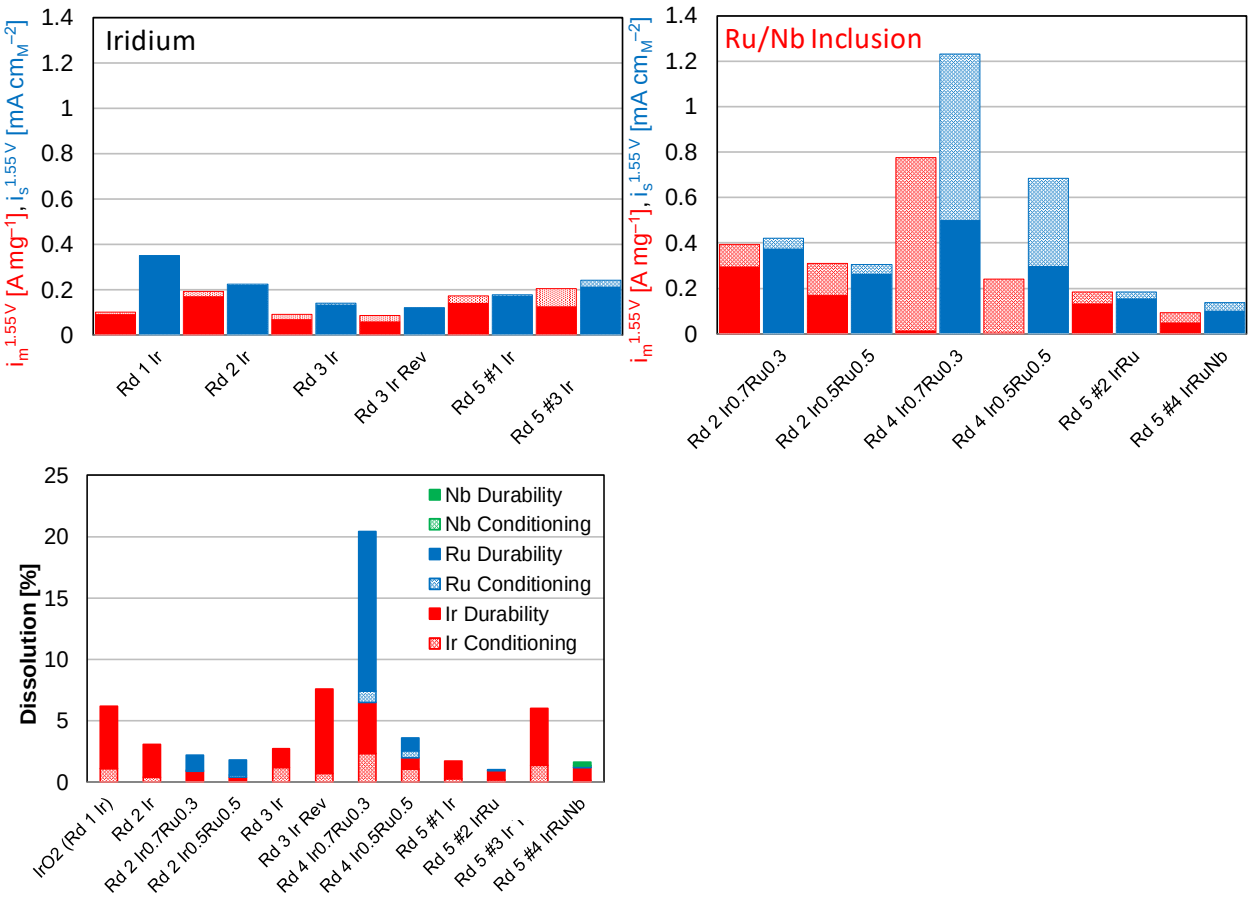

Figure 33. Mass (red) and specific (blue) OER activities of screened catalysts prior to (shaded) and following (solid) stability testing (13.5 h at 2 V), separated based on materials that (a) contained only Ir or (b) including ruthenium. (c) Catalyst dissolution prior to (shaded) and following (solid) stability testing for Ir (red), ruthenium (blue), and niobium (green). Dissolution was calculated by ICP-MS and the known catalyst loading and electrolyte volume.

Following rotating disk electrode stability testing, surface areas were also evaluated with hydrogen underpotential deposition and capacitance to qualitatively evaluate changes to the metal/oxide content (**Figure 34**). Compared to the initial performance, most catalysts saw lower hydrogen underpotential deposition response, or a drop-in metal contribution. A drop-in capacitance was also common, consistent with catalyst dissolution and material loss. In certain instances, the capacitance grew and indicated oxide growth. As with ECA measurements initially, differences between HUPD/capacitance and mercury underpotential deposition were reflective of mixed oxides, where the surface was not entirely metallic (to increase the HUPD response) and not an oxide throughout (to increase the capacitance).

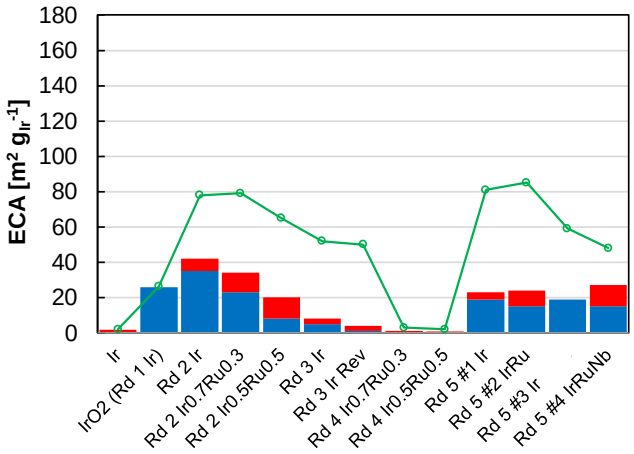

Figure 34. ECAs of screened catalysts following stability testing (13.5 h at 2 V), including the responses from hydrogen underpotential deposition (HUPD, red), capacitance (blue), and mercury underpotential deposition (HgUPD, green).

Based on learnings from Nel an NREL's collaborative work on catalyst preparation, regarding the impact of catalyst properties (surface area, particle morphology, etc.) and composition (pure IrOx compounds vs. blended metal oxides), catalyst candidates were procured from two commercial companies able to produce catalyst materials in kilogram quantities. Iridium oxide with high surface area was obtained from both companies, while the second company also provided different blends of ruthenium for activity and niobium for stability. Materials were integrated with Nel's ink formulations and deposition processes and tested for initial performance (**Figure 35**).

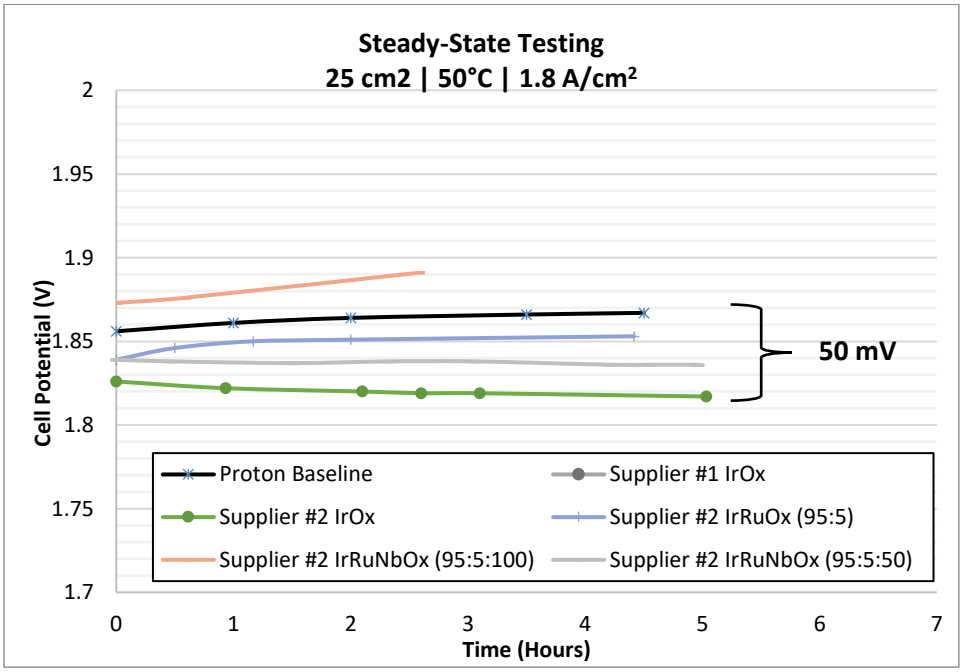

Figure 35: Catalyst screening data

Both IrOx materials performed better than the Nel baseline on this short-term test, but Supplier #2 showed the best performance. The blended catalysts also performed relatively well, except

for the catalyst with high niobium content, indicating the non-active material dominated the catalyst properties. The three best performing candidates from Supplier #2 were incorporated into new electrodes for the longer-term milestone test.

Task 4: Validation and Program Management

Key Findings: Advanced Catalyst

- End of program goal was to achieve 500hrs of durability at a loading of 0.9 mg/cm^2 for the OER electrode, this was exceeded through stable operation over 1500hrs at a loading of 0.7 mg/cm^2. This represents an 80% reduction in PGM loading for the CCM versus the Nel baseline.
- In addition to the successful achievement for the end of program milestone, this was achieved with a catalyst composition of IrRuOx developed under this funding agreement, which also is cheaper than pure IrOx due to the lower cost ruthenium content added for improved activity.
- The incorporation of these alternative manufacturing methods enabled the use of a 50-micron membrane, which resulted in an ~66% reduction in membrane thickness and material used. Use of this membrane serves to reduce both operating expense and capital expense.

Based on the membrane work and integrating these three catalyst materials, a 3-cell stack was assembled for testing under standard and aggressive conditions. Of note, loadings for the original test were 3.0 mg/cm^2 on the anode (OER) and 3.0 mg/cm^2 for the cathode (HER), using PtBlack. For this end of program milestone, not only were these alternative OER catalysts incorporated, but the cathode was modified as well, with a transition from PtBlack to Pt/C. This enabled our first opportunity to explore lower loadings under this program with successful processing at a loading of 0.3 mg/cm^2. This represented an order of magnitude reduction of PGM content on the HER side of the cell. Once assembled and placed on test, operation was performed at 30 bar differential pressure. Initially, the stack was operated at Nel's standard commercial conditions of 50°C and 1.8 A/cm^2. After the first 500 hours, the stack temperature was increased to 80°C, and after another 150 hours the current was increased by 20%. The stack was operated for over 1400 hours before being removed for a replicate test which is ongoing. The metric for the milestone was to achieve less than 4 microvolts per hour and over 500 hours of operation. The decay rates for the two best performing catalysts are shown in the trendlines in the Figure. The last 500 hours of the test were used to calculate the decay rate because the data was relatively flat throughout, and any degradation would be expected to be worse at the most aggressive conditions. Also, if the catalyst is degrading, the decay rate often increases with operation as the amount of active material decreases and the remaining catalyst material is under higher demand. Finally, there can also be minor fluctuations in early stack operation due to break in processes which could have skewed the data. The high surface iridium oxide material actually had a slightly negative apparent decay rate. Nel has observed this behavior in other stacks and hypothesized that the improvement could be due to compression and improved contact of the components under the stack load, or other break in effects. The lack of observable decay indicates that the catalyst is very stable and meets the milestone. The blended Ir-Ru catalyst also showed a low decay rate of 5 microvolts per hour, which is within the experimental error over this period of performance. Longer runtime would provide higher precision of the measurement, but the data collected during this final test meets the final programmatic targets.

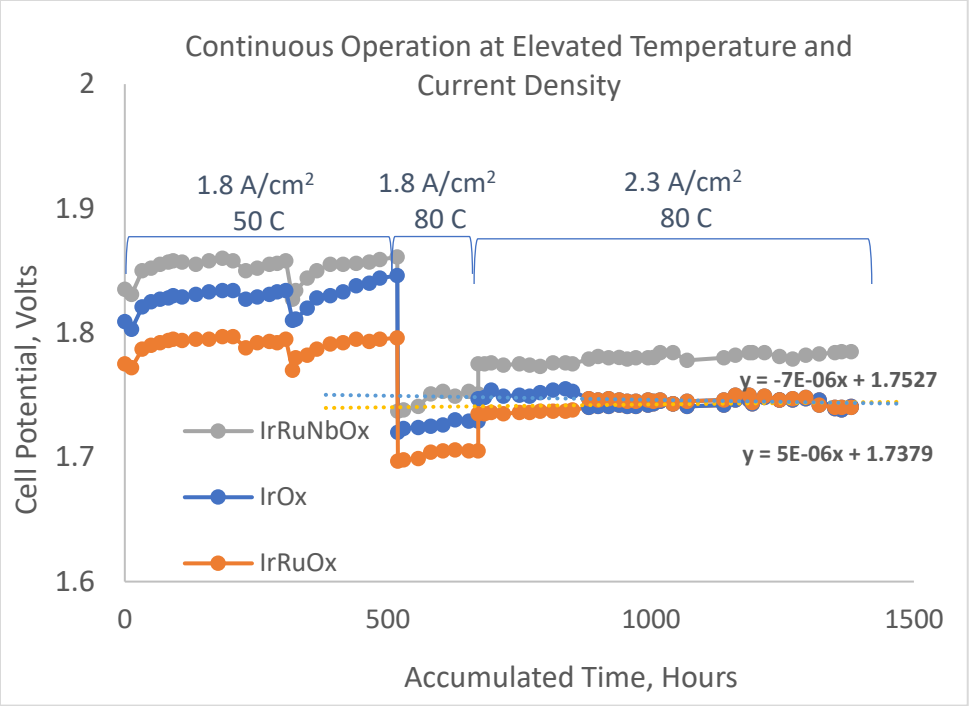

Figure 36: Steady-state data of high efficiency MEA for Go/No-Go milestone

Regular correspondence and meetings took place over the entirety of the project to discuss progress and material needs between partners and nodes. Subsequently, weekly meetings have been held at Proton for internal planning and material preparation for test and milestone completion. All milestones were completed, and quarterly reports submitted by all team partners.

Conclusions:

All program milestones were met successfully with partner contributions providing required configuration inputs to the final end of program deliverable. While the end of program goal was to achieve 500hrs of durability at a loading of 0.9 mg/cm^2 for the OER electrode, this was exceeded through stable operation over 1500hrs at a loading of 0.7 mg/cm^2. In addition to the successful achievement for the end of program milestone, this was achieved with a catalyst composition of IrRuOx developed under this funding agreement, which also is cheaper than pure IrOx due to the lower cost ruthenium content added for improved activity.

In addition, an effective cross-over mitigation strategy was developed to scavenge hydrogen diffusion to the anode. Project requirements had a target of 75% effectiveness, but 87% was demonstrated in full system turndown. As a final output from the effort, design changes and alternative methods of electrode manufacture where developed. The incorporation of these manufacturing methods enabled the use of a 50-micron membrane, which resulted in an ~66% reduction in membrane thickness versus the current commercial design at Nel. This end result will translate into both a capital cost reduction, as well as a lower operating expense through lessening of ohmic resistance.

Issues: Covid-19 delayed Nel and project partners

- No-cost extensions were received to accommodate these delays.

Patents: None

Publications / Presentations:

K. E. Ayers, W. L. Gellett, and C. B. Capuano, "Electrochemical Generation of Fuels: Matching Research and Application for Advanced Water Splitting and Other Technologies", Spring ECS 2018 (presentation)

K. Ayers and C. Capuano, "High Efficiency PEM Water Electrolysis Enabled by Advanced Catalysts, Membranes and Processes", DOE AMR 2018 (presentation)

K. Ayers and C. Capuano, "High Efficiency PEM Water Electrolysis Enabled by Advanced Catalysts, Membranes and Processes", ECS Fall 2018 (presentation)

K. Ayers and C. Capuano, "High Efficiency PEM Water Electrolysis Enabled by Advanced Catalysts, Membranes and Processes", DOE AMR 2019 (presentation)

K. Ayers and C. Capuano, "High Efficiency PEM Water Electrolysis Enabled by Advanced Catalysts, Membranes and Processes", ECS Fall 2019 (presentation)

Leonard, Emily, Shum, Andrew D., Danilovic, Nemanja, Capuano, Christopher, Ayers, Katherine E., Pant, Lalit M., Weber, Adam Z., Xiao, Xianghui, Parkinson, Dilworth Y., and Zenyuk, Iryna V. Interfacial analysis of a PEM electrolyzer using X-ray computed tomography. United States: N. p., 2019. Web. doi:10.1039/c9se00364a.

Creel Erin Brahm, Lyu Xiang, McCool Geoff, Ouimet Ryan J., Serov Alexey. Protocol for Screening Water Oxidation or Reduction Electrocatalyst Activity in a Three-Electrode Cell for Alkaline Exchange Membrane Electrolysis. Frontiers in Energy Research, 10, 2022. 10.3389/fenrg.2022.871604.

Pongsarun Satjaritanun, Maeve O'Brien, Devashish Kulkarni, Sirivatch Shimpalee, Cristopher Capuano, Katherine E. Ayers, Nemanja Danilovic, Dilworth Y. Parkinson, Iryna V. Zenyuk. Observation of Preferential Pathways for Oxygen Removal through Porous Transport Layers of Polymer Electrolyte Water Electrolyzers. iScience, Volume 23, Issue 12, 2020, doi.org/10.1016/j.isci.2020.101783.

Devashish Kulkarni, Alex Huynh, Pongsarun Satjaritanun, Maeve O'Brien, Sirivatch Shimpalee, Dilworth Parkinson, Pavel Shevchenko, Francesco DeCarlo, Nemanja Danilovic, Katherine E. Ayers, Christopher Capuano, Iryna V. Zenyuk. Elucidating effects of catalyst loadings and porous transport layer morphologies on operation of proton exchange membrane water electrolyzers. Applied Catalysis B: Environmental, Volume 308, 2022, doi.org/10.1016/j.apcatb.2022.121213.

Milestone Schedule

Milestone #	Project Milestones	Type	Task Completion Date (Project Quarter)				Progress Notes
			Original Planned	Revised Planned	Actual	Percent Complete	
1.2.1	Provide an initial short list of downselected membranes and hydration conditions (up to 4 in combination) and ranked likelihood for final downselect based on mechanical stability and hydration results, with a minimum tensile strength of 20 MPa, elongation to break of 150%, and maximum water uptake of 50%.	Milestone	6/30/18		6/30/18	100%	**Completed**. Analysis completed and focus on N117 and Solvay 90 µm downselect.
2.1.1	Procurement, fabrication of MEAs, and baseline testing of at least 3 advanced catalysts and 3 ink formulations, with at least one MEA meeting cell performance of 1.85V at 1.8 A/cm^2 using N117 membrane	Milestone	3/31/18		3/31/18	100%	**Completed**. 4 catalysts synthesized for OER testing have been operationally tested at Proton and characterized by NREL. **Performance target met, and milestone achieved**.
2.2.1	Quantify the morphology and water distribution for interfaces and individual cell components using XCT, and provide a strategy for performance optimization (define areas of risk and mitigation) through combination of membrane type, electrode fabrication parameters, and operating conditions	Milestone	6/30/18		6/30/18	100%	**Completed**. Tufts has conducted a fourth round of image analysis, which was provided to LBL. High current density achieved, and variations shown between configurations. Results used and verified in model at LBL for PEMWE
3.1.1	Define potential efficiency benefit from combined nanoparticle structure and catalyst composition and provide strategy for catalyst powder optimization in BP 2 (higher focus on alloys or Ire structure).	Milestone	9/30/18		9/30/18	100%	**Completed**. Samples synthesized, characterized, and tested showing influence of oxides versus metal content on dissolution and activity. Composition used for final milestone and future optimization
Go/No-Go #1	**Demonstrate capability to meet the MEA Specific Project Targets given in Table 1 using advanced MEA components (e.g., membrane, catalyst) developed in this project at 80-90oC. Also, demonstrate performance of this advanced MEA of 1.8 A/cm^2 at ≤1.7 V.**	**Go/No-Go**	**9/30/18**		**7/15/18**	**100%**	**Completed. Milestone achieved with <1.7V performance met with down-selected membrane and OER catalysts synthesized at Proton**
4.2.1	Develop project target tracking sheet based on preliminary data. Define baseline current hydrogen costs based on the current cell configuration, to be updated as the project progresses	Milestone	12/31/17		12/31/17	100%	**Completed**. Project Gantt chart and performance tracker submitted to DOE technology manager and approved

Milestone #	Project Milestones	Type	Task Completion Date (Project Quarter)				Progress Notes
			Original Planned	Revised Planned	Actual	Percent Complete	
1.2.2	Understand impact of membrane hydration conditions for 3 membrane candidates across a temperature range of 50°C to 100°C and quantify changes in compressive strength and MEA efficiency over the temperature range.	Milestone	12/31/2018		12/31/2018	100%	**Completed**. Analysis completed and differences in water content versus in-cell performance measured.
1.2.3	Down-select membrane based on hydration state study of mechanical and chemical properties. Membrane selection will be determined by loss of compressive strength of no more than 20% vs. baseline membrane and hydration conditions, and optimal efficiency among membranes meeting the strength metric	Milestone	3/31/2019		3/31/2019	100%	**Completed.** Less than 10% loss observed in mechanical properties for Nafion and Solvay resulting from hydration and processing conditions as measured at LBL
2.2.2	In-operando electrolysis cell is operational and two best of the class MEAs are characterized under two current densities of 500 and 1000 mA/cm^2.	Milestone	6/30/19		6/30/2019	100%	**Completed.** Up to $4A/cm^2$ current density achieved and evaluated. Both fiber and particle PTLs assessed. CCM and GDE worked well with particle PTL and sintered in terms of performance and flow distribution
Go/No-Go #2	**Using advanced MEA components (e.g., membranes, catalysts) developed in this project, demonstrate 500 hr durability using steady state or AST of target advanced MEA at > 80 ºC compared to baseline, achieving a degradation rate of <4 mV/1000 hr.**	**Go/No-Go**	**9/30/19**		**8/30/2019**	**100%**	**Completed.** Results in this report. Durability target achieved.
1.3.1	Downselect crossover mitigation using operational data and TEM characterization. H_2 recombination effectiveness should be >75% based on initial crossover current for untreated membrane vs. treated membrane. TEM should show particles isolated from the anode catalyst layer, and particles should be retained in membrane after 1000-hour test.	Milestone	12/31/2019		12/20/2019	100%	**Completed.** Results in this report. Durability target achieved.
2.2.3	Ex-situ and in-operando data are fed into deterministic contact mechanics model and directly meshed, and resistances are extracted. The results are delivered to LBNL for cell performance modeling.	Milestone	3/31/2020			100%	Completed. CCM and PTE testing results from UCI have been shared with LBNL.

Milestone #	Project Milestones	Type	Task Completion Date (Project Quarter)				Progress Notes
			Original Planned	Revised Planned	Actual	Percent Complete	
4.2.1	Provide Hydrogen with advanced MEA for validation based on 500 hr durability downselect, as discussed above. The advanced MEA will consist of components (e.g., membranes, catalysts) developed in this project, demonstrating 500 hr durability using steady state or AST of target advanced MEA at > 80 °C compared to baseline, achieving a degradation rate of <4 mV/1000 hr. Total electrode PGM content will be 0.9 mg/cm^2 with final down-selected hydrogen cross-over mitigation included	Milestone	6/30/2020			100%	**Complete**. All testing conducted at Nel for final test in commercial hardware per Dave P.
End of Project Goal	Demonstrate activity and 500 hr durability of advanced MEA in 3-cell 86 cm^2 electrolysis stack that meets all the project specific targets given in Table 1	End of Project Goal	8/31/2020			100%	**Complete**. Exceeded 1000 hrs target. Catalyst loading reductions applied and represent an achievement beyond project requirements